Adjustment of Offshore Flow

Larry Mahrt

College of Oceanic and Atmospheric Sciences

Oregon State University

Corvallis, OR 97331

phone: (541) 737-5691 fax: (541) 737-2540 email: mahrt@oce.orst.edu

Grant #: N000140010121

http://blg.oce.orst.edu/rasex

FINAL REPORT
17 SEPTEMBER 2001

REPORT DOCUMENTATION PAGE

Form Approved
OMB No. 0704-0188

1. REPORT DATE *(DD-MM-YYYY)*	2. REPORT TYPE	3. DATES COVERED *(From - To)*
17-09-2001	Final Report	15/11/1999 - 31/10/2001

4. TITLE AND SUBTITLE

Adjustment of Offshore Flow

5a. CONTRACT NUMBER

5b. GRANT NUMBER

N000140010121

5c. PROGRAM ELEMENT NUMBER

6. AUTHOR(S)

Mahrt, Larry

5d. PROJECT NUMBER

5e. TASK NUMBER

5f. WORK UNIT NUMBER

7. PERFORMING ORGANIZATION NAME(S) AND ADDRESS(ES)

Oregon State University
312 Kerr Admin Bldg
Corvallis OR 97331-2140

8. PERFORMING ORGANIZATION REPORT NUMBER

9. SPONSORING/MONITORING AGENCY NAME(S) AND ADDRESS(ES)

Office of Naval Research
Ballston Centre Tower Cone
800 N Quincy St
Arlington VA 22217-5660

10. SPONSOR/MONITOR'S ACRONYM(S)

11. SPONSORING/MONITORING AGENCY REPORT NUMBER

12. DISTRIBUTION AVAILABILITY STATEMENT

Approved for Public Release; Distribution is Unlimited

13. SUPPLEMENTARY NOTES

14. ABSTRACT

We have analyzed a variety of offshore data sets to study the fluxes of heat and momentum between the sea surface and the atmosphere in the coastal zone. We have found that the vertical structure of atmospheric offshore flow is much more complex than previously thought, especially in the case of advection of warm air from land over cooler water. We have developed new formulations for modeling sea surface fluxes. Modification of computer models to predict the atmospheric structure in the coastal zone requires more work for cases of complex seas and warm air over cooler water. The previous success of the Charnock formulation in the literature may have also been primarily due to artificial self-correlation rather than real physical effects.

15. SUBJECT TERMS

offshore flow, internal boundary layers, surface fluxes

16. SECURITY CLASSIFICATION OF:			17. LIMITATION OF ABSTRACT	18. NUMBER OF PAGES	19a. NAME OF RESPONSIBLE PERSON
a. REPORT	b. ABSTRACT	c. THIS PAGE			Larry Mahrt
					19b. TELEPONE NUMBER *(Include area code)* (541) 737-5691

Adjustment of Offshore Flow

Larry Mahrt

College of Oceanic and Atmospheric Sciences

Oregon State University

Corvallis, OR 97331

phone: (541) 737-5691 fax: (541) 737-2540 email: mahrt@oce.orst.edu

Grant #: N000140010121

http://blg.oce.orst.edu/rasex

FINAL REPORT
17 SEPTEMBER 2001

Adjustment of Offshore Flow

Final Report

Larry Mahrt
College of Oceanic and Atmospheric Sciences
Oregon State University
Corvallis, OR 97331
phone: (541) 737-5691 fax: (541) 737-2540 email: mahrt@oce.orst.edu
Grant #: N000140010121
http://blg.oce.orst.edu/rasex

LONG-TERM GOAL

Derive a new drag law and roughness length relationship for the coastal zone.

OBJECTIVES

Our primary objective is to isolate the influences of wave age and fetch on the drag coefficient and surface roughness length. This includes examination of the influence of internal boundary layer development on heat and momentum fluxes in the coastal zone, that can lead to large deviations from existing similarity theory. The second main objective is to augment the wave age with more specific wave properties. The final objective is to provide the data sets to other modeling groups.

APPROACH

Our initial objectives were realized by first quality-controlling the RASEX data and intercomparing fluxes between different levels. Different estimates of the "observed" roughness length using the profile and eddy correlation methods were compared. Using the observed values of the drag coefficient and roughness height, different existing relationships were tested and new formulations for the transfer coefficients for heat and momentum were developed. The analysis has been extended to a much larger RASEX data set outside the intensive period, which includes a large sample of offshore internal boundary layer cases. We have also added the offshore tower data from the University of Uppsala.

WORK COMPLETED

During the past year, we have evaluated the Charnock relationship and simple wave age models using RASEX and the Swedish data sets. We have also explored the relationship between the aerodynamic roughness length and atmospheric stability.

RESULTS

The Charnock coefficient relates the aerodynamic roughness length to the surface friction velocity. To our surprise, we found that the success of the Charnock relationship is almost exclusively due to artificial correlation guarenteed by the relationship between the friction velocity and the roughness length in the Monin-Obukhov drag law (stability-modified log law). In fact a higher order parameterization of the roughness length in terms of the friction velocity out performs the Charnock relationship, although the success of this formulation is due primarily to artificial correlation as well. These results were suggested by both the random rearrangement of actual values of the input variables

(heat flux, wind speed and momentum flux) and by specifying a gaussian distribution of each independent variable.

We have found that the aerodynamic roughness length depends substantially on atmospheric stability. The roughness length is orders of magnitude smaller with stable conditions, presumably due to supression of downward momentum transport to the sea surface is weaker. This stability dependence also leads to a stability dependence of the Charnock coefficient (Figure 1). For these analyses, the RASEX data did not contain a sufficiently wide range of stability to assess the stability dependence. We therefore supplimented the Swedish data sets with existing data sets which we have in-house.

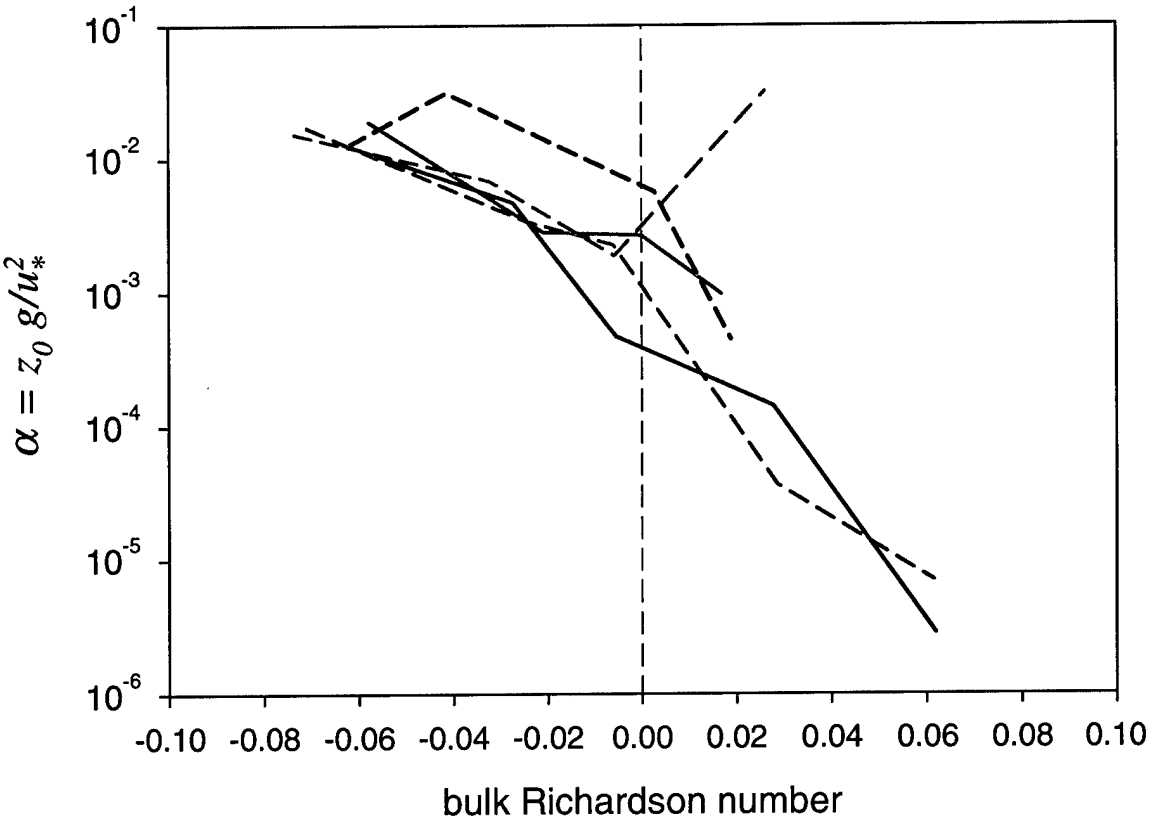

Figure 1. The dependence of the Charnock coefficient on the bulk Richardson number defined in terms of the temperature and wind at the observational level and the sea-surface temperature. The data sets are the Swedish 8-m data from an offshore tower in the Baltic (red solid), LongEZ aircraft data from approximately 15 m during SHOWEX (November 1997-black dashed, March 1999-blue solid, November 1999-red dashed) and TOAGA COARE NCAR Electra data at approximately 30 m (green dashed),

All the data sets indicate a similar decrease of the Charnock coefficient with increasing stability except for the TOAGA COARE data. In the latter data set, significant stability is achieved by very weak winds rather than significant air-sea temperature difference. Furthermore, the number of cases is fairly small because of the minimum wind speed criteria.

However, we have not yet reached a decision on whether a formulation of a stability dependent roughness length or Charnock coefficient is ready for use in models where no information on wave state is available. This stability dependence is different between weak wind and moderate wind

conditions, persumably due to the increased influence of swell with weak winds. The composited results in Figure 1 exclude winds less than 4 m/s. More investigation is needed.

We have also developed models of the roughness length and Charnock coefficient on wave age. Again, the resulting relationship is largely due to artificial self-correlation. We are currently studying the influence of swell propagation with respect to the mean wind.

IMPACT/APPLICATION

The previous success of the Charnock formulation in the literature may have also been primarily due to artificial self-correlation. This does not suggest that common use of the Charnock formulation in numerical models should be terminated but rather that existing physical interpretation of the Charnock formulation cannot be justified. In addition, the common use of the Charnock relationship to reduce the drag coefficient to neutral values is not justified and may lead to misleading results.

RELATED PROJECTS

Work on an ONR grant entitled "Spatial Variations of the Wave, Stress and Wind Fields in the Shoaling Zone" (N00014-97-1-0279) has completed the observational work and is concentrating on data analysis. This program studies spatial variations in the coastal zone using the LongEZ research aircraft and ground based sonic anemometers at the shore and on the pier.

PUBLICATIONS

Mahrt, L., D. Vickers, J. Edson, J. Wilczak, J. Hare and J. Hojstrup, 2001. Vertical structure of offshore flow during RASEX. Boundary-Layer Meteorology, **100**, 47-61.

VERTICAL STRUCTURE OF TURBULENCE IN OFFSHORE FLOW DURING RASEX

A. L. Mahrt (mahrt@oce.orst.edu)
College of Oceanic and Atmospheric Sciences, Oregon State University,Corvallis, OR 97331, U.S.A.

B. Dean Vickers
College of Oceanic and Atmospheric Sciences, Oregon State University,Corvallis, OR 97331, U.S.A.

C. Jim Edson
Woods Hole Oceanographic Institute, Woods Hole, MA 02543, U.S.A.

D. James M. Wilczak
Environmental Technology Lab., ERL/NOAA, Boulder, CO 80303, U.S.A.

E. Jeff Hare
Cooperative Institute for Research in Environmental Sciences (CIRES), University of Colorado and Environmental Technology Lab., ERL/NOAA, Boulder, CO 80303, U.S.A.

F. Jørgen Højstrup
RisøNational Laboratory, 4000 Roskilde, Denmark

Abstract. The adjustment of the boundary layer immediately downstream from a coastline is examined based on two levels of eddy correlation data collected on a mast at the shore and six levels of eddy correlation data and profiles of mean variables collected from a mast 2 km offshore during RASEX. The characteristics of offshore flow are studied in terms of case studies and inter-variable relationships for the entire one month data set. A turbulent kinetic energy budget is constructed for each case study.

The buoyancy-generation of turbulence is small compared to shear-generation and dissipation. However, weakly stable and weakly unstable cases exhibit completely different vertical structure. With flow of warm air from land over cooler water, modest buoyancy destruction of turbulence and reduced shear-generation of turbulence over the less-rough sea surface cause the turbulence to rapidly weaken downstream from the coast. The reduction of downward mixing of momentum by the stratification leads to smaller roughness lengths compared to the unstable case. Shear-generation at higher levels and advection of stronger turbulence from land often lead to a maximum of stress and turbulence energy above the surface and downward transport of turbulence energy toward the surface.

With flow of cool air over a warmer sea surface, a convective internal boundary layer develops downstream from the coast. An overlying relatively thick layer of downward buoyancy flux (virtual temperature flux) is sometimes maintained by shear-generation in the accelerating offshore flow.

Keywords: Coastal zone, Air-sea interaction, Sea surface stress, Internal boundary layer, Turbulence energy.

1. Introduction

The response of the atmosphere to surface discontinuities is often posed in terms of internal boundary layers (Garratt, 1990). In flow of warm air from a rough land surface over a cooler sea surface, the turbulence decreases due to a combination of stable stratification over the water and reduced surface roughness. The flow above the thin stable surface layer, which was part of the boundary layer over land, may become partially decoupled from the surface, accelerate and form a low-level wind maximum (Smedman et al., 1995; Tjernström and Smedman, 1993). The shear on the underside of the low-level wind maximum may eventually generate turbulence and reestablish a surface-based boundary layer. In this case, the main source of turbulence is elevated and not at the surface and Monin-Obukhov scaling does not apply (Smedman et al., 1995). Sun et al. (2000) show that close to the coast, advection from land dominates the near-surface stress.

Even without such decoupling, the reduction of surface roughness and surface stress over the sea can lead to a low-level wind maximum in offshore flow of warm air over cooler water (Garratt and Ryan, 1989). In a numerical study of the influence of the continental diurnal variation on offshore flow, Garratt (1987) found that the onset of daytime convective turbulence was advected offshore as a sharp horizontal change that could be traced for hundreds of kilometers offshore, well beyond the fetch in the present data. The numerical simulations of Mengelkamp (1991) indicate that the top of the stable internal boundary layer can be defined in terms of a minimum in the vertical profile of turbulence kinetic energy while numerical simulations of Garratt (1987) similarly indicate a minimum of eddy diffusivity at the top of the stable internal boundary layer. The level of minimum turbulence separates the underlying internal boundary layer from overlying decaying turbulence. In Mengelkamp (1991), this overlying decaying turbulence still exhibits some upward buoyancy flux offshore, characteristic of the upstream convective boundary layer.

A number of studies document development of well-defined convective internal boundary layers in flow of cool air over a warm surface (see review in Garratt, 1990). The growing convective internal boundary layer is capped by a thin entrainment zone of downward buoyancy flux. In contrast, Sun et al. (1998) studied a convective internal boundary layer, which is capped by a relatively thick layer of downward buoyancy flux, maintained by elevated shear-generation. The above studies suggest varied vertical structure of the convective internal boundary layer in offshore flow.

The present study analyses offshore data from the Risø Air-Sea Experiment (RASEX). Using this data, Vickers and Mahrt (1999) found that close to the coast, modifications to Monin-Obukhov similarity theory may be required. Convective eddies are suppressed by the top of the thin internal boundary layer in unstable offshore flow. This partial suppression leads to larger nondimensional gradients and weaker fluxes than predicted by Monin-Obukhov similarity theory. For stable offshore flow, the nondimensional shear is smaller than predicted by the usual stability functions for Monin-Obkuhov similarity theory, particularly for young waves. In contrast, above the wave boundary layer for stationary onshore flow, Monin-Obukhov scaling successfully describes the turbulence energy budget (Edson and Fairall., 1998; Wilczak et al, 1999) and the flux- gradient relationship (Vickers and Mahrt, 1999).

2. Data

We analyze offshore tower data collected during RASEX. The full instrumentation is described in Barthelmie et al. (1994) and Højstrup et al. (1997). In this study, we analyze observations taken at the sea mast west tower, located 2 km off the northwestern coast of the island of Lolland, Denmark, in 4 m of water, for the intensive observing period 3 October through 8 November 1994. The variation in mean water depth due to tides is only about 0.3 m. Local off-shore (southerly) flow is characterized by a sea fetch ranging between 2 km and 5 km. On-shore flow has a fetch between 15 km and 25 km as it travels across an inland sea, and is still potentially fetch-limited. Fetch is the distance along the flow from the coast to the sea mast. Water depths for the longer fetches range from 4 m to 20 m. The nearby land surface is relatively flat farmland.

Various corrections to the data are recorded in Mahrt et al. (1996). Averaged vertical profiles of the buoyancy flux and friction velocity are computed from the six levels of sonic anemometers. In offshore flow, the vertical variation of the flux is much larger than differences between individual sonic anemometers. For some analyses, the fluxes for the three lowest levels will be averaged since the effect of instrumental differences may be larger than the actual vertical variation over such short vertical distances. The stability z/L for each record is computed from the fluxes averaged over the three lowest levels, where L is the Obukhov length. Insight into the vertical structure of the offshore flow can be gained by evaluating the turbulence kinetic energy budget using the stress and virtual temperature flux computed from sonic anemometers located at 3, 6, 10, 18, 32 and 45 m on the offshore tower.

For shear-generation of turbulence kinetic energy, the mean wind shear is computed from seven cup anemometers (P224b sensor) located at 7, 15, 20, 29, 38, 43 and 48 m. Corrections to the cup anemometers were made by compositing the wind speed profile based on all of the records with fetch greater than 10 km and near-neutral conditions (abs.(z/L) $<$ 0.1). This averaged profile is fit to a log-linear height-dependence and percentage corrections for each level are constructed from the deviation of the averaged profile from the log-linear fit. These corrections partially remove small systematic irregularities in the profile due to instrument error. Percentage corrections to the wind speed are always less than 2% but exert a greater influence on the shear. The computation of the shear-generation term neglects directional shear, which could not be adequately estimated from the sonic anemometer data due to small uncertainties in orientation.

For offshore cases (fetch $< 5km$), advection of turbulence kinetic energy is estimated as

$$V[\frac{TKE_{SM} - TKE_{LM}}{fetch}] \tag{1}$$

where SM refers to the offshore mast and LM refers to the land mast. This term can be estimated at the 6- and 18-m levels, corresponding to the common sonic anemometer levels at the landmast and seamast. The wind speed V is the taken from the appropriate level at the sea mast Here, it is assumed that the turbulence kinetic energy, TKE, is spatially invariant along the coast for cases where the flow was not perpendicular to the coast. The above estimate of advection is probably an upper bound for the tower since the gradients are presumably strongest closer to the coast. Unfortunately, advection could not be estimated above 18 m.

Dissipation is estimated following the spectral approach of Edson and Fairall (1998). The spectral slope was determined from a least squares fit over the frequency range thought to be in the inertial subrange. In some cases, the inertial subrange does not appear to be fully developed possibly due to nonequilibrium conditions in offshore flow and errors in the dissipation estimate may be significant. We expect the wave-induced pressure transport term to be small for this data even at the lowest (3 m) tower level (Hare et al., 1997). The wavelength and amplitude of the fetch-limited surface waves are generally small compared to open ocean values.

The residuals for the turbulence kinetic energy budget are expected to be large because the pressure transport term is neglected and the errors in the vertical flux divergence and horizontal advection of turbulence energy are expected to be significant. The vertical flux divergence

of turbulence energy (triple correlation term) suffers larger random flux errors compared to covariances, and the flux divergence term is a small difference between vertical flux of turbulence energy at two levels. We have also neglected the Eulerian time-dependence term, the mean vertical advection of turbulence kinetic energy as well as horizontal flux divergence of turbulence energy equation. These terms appear to be small with relatively large errors.

3. Land-sea contrast

The maximum upward buoyancy flux at the sea surface most often occurs in the morning when the air advected from the land is coolest. The maximum downward buoyancy flux at the sea surface tends to occur in the late afternoon when the air over land is warmest. On average, the diurnal amplitude of the buoyancy flux is 0.02 $^{\circ}Cms^{-1}$. This averaged diurnal amplitude is small due to the low sun angle for 54 N in October and inclusion of numerous cloudy days in the average. Using temperature at two levels for summer for the same land and sea masts, Barthelmie et al. (1996) found, on average, stable conditions over the water during the day and unstable conditions at night.

For the data analyzed here, the stress at the seamast in offshore flow is on average half of the value over land. The flow typically accelerates $1 - 2ms^{-1}$ between land and the offshore mast. The roughness lengths over land (Barthelmie et al., 1996) are approximately 10 cm for southerly (offshore flow) and 5 cm for south easterly flow where trajectories experience a mixture of land and sea. These roughness lengths are several orders of magnitude larger than those over the sea.

The buoyancy fluxes are relatively weak in this data set and the magnitude of z/L only occasionally exceeds 0.5. None the less, the vertical structure of the flow is sensitive to whether the flow is weakly unstable or weakly stable. The greater sensitivity of the flow to stability compared to over land (Section 5) may be due to coupling between the roughness length over the sea and the stability, as found in Plant et al. (1998). With stable conditions, the momentum flux to the sea surface is weaker. This corresponds to slower wave growth and smaller roughness compared to near-neutral and unstable cases.

To examine this relationship for the present data, roughness lengths were computed from the observed fluxes from individual one-hour records using the Paulson-Dyer stability functions. The roughness lengths were then averaged for different intervals of z/L. As a second calculation, roughness lengths were computed from fluxes, which were first averaged for different intervals of z/L before computing the roughness length.

Both methods showed a sharp decrease of the roughness length with increasing stability. For the second method, the roughness length for offshore flow at 3 m decreases from 0.05 cm for near-neutral conditions to 0.003 cm for the stability interval centered on $z/L = 0.2$, to 0.001 cm for the stability interval centered on $z/L = 0.6$. The corresponding Charnock coefficient is 0.015 for near neutral conditions, close to traditional values. The values of the Charnock coefficient decreases to near smooth flow values for the stable categories. As a result, the influences of stability and roughness change on the offshore flow are coupled and the over all effect of stability is enhanced compared to that over land. This problem is currently being investigated with eddy correlation and wave data from multiple sites. Inaccuracy of the Dyer stability function does not seem to be the cause of the correlation between the roughness lengths and stability.

For the relationships examined in subsequent sections, the characteristics of the offshore flow are more systematically related to travel time than fetch in terms of the scatter, suggesting that the flow is influenced by an internal decay time scale. The turbulence may decay more near the surface where the travel time to the tower is longer (weaker wind near the surface) and the dissipation time scale is shorter (smaller turbulent length scale near the surface). For offshore flow, the travel times at the offshore mast generally range between a few hundred seconds and about 600 seconds. The decay time of convective turbulence can be estimated in terms of the ratio of the vertical length scale of the turbulence divided by the velocity scale of the turbulence. Nieuwstadt and Brost (1986) and Sorbjan (1997) provide specific formulations for the case where the velocity scale is the free convection velocity and the length scale is the depth of the convective mixed layer. Applying such a relationship to the RASEX cases with convective conditions over land predicts a decay time scale on the "order" of ten minutes, which is consistent with the observed variation of turbulence quantities with travel time over the sea found in Sections 4-5.

4. Upward buoyancy flux from the sea surface

We now study the flow of cool air over the warmer sea surface in terms of three periods when the buoyancy flux at the surface exceeds 0.01 $^{\circ}Cms^{-1}$ for more than a half day (Table 1). All three cases are characterized by very weak instability. The time-height cross-section for the case of longest duration (Figure 1) shows diurnal variation with maximum upward buoyancy flux in the morning due to advection of cool air from land.

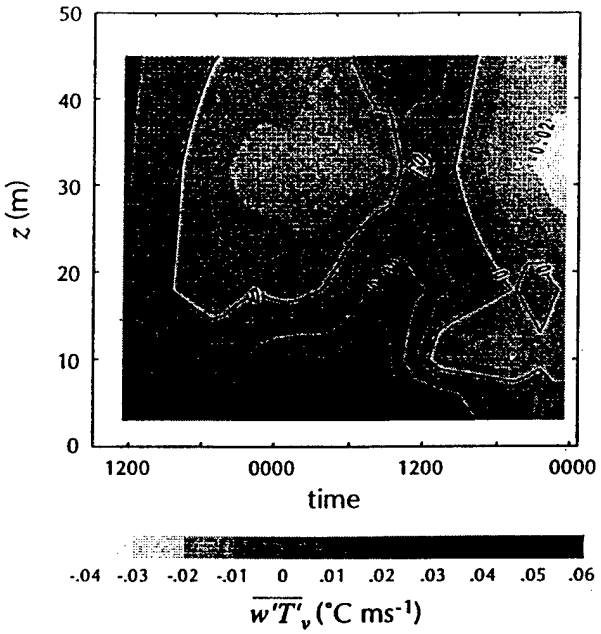

Figure 1. Time-height cross-section for unstable case UI for the buoyancy flux ($°Cms^{-1}$) where darker areas correspond to upward buoyancy flux. Times are GMT which is one hour behind local solar time.

The turbulence energy budget is averaged over all of the one-hour Records within each case. Averaging over nonstationary periods does not correspond to an ensemble average. However, the individual one-hour budgets are noisier especially with respect to the smaller terms in the turbulence kinetic energy budget. The residuals of the averaged turbulence energy budgets (Figure 2) are reasonably small considering the possible substantial errors in certain terms of the budget and omission of the pressure transport term (Section 2). Error bars for the averaged profiles are not shown because much of the variation within the averaging period is due to either diurnal trend or other nonstationarity, rather than random variations. The analysis in this section also considers statistics based on all of the individual one-hour records within the entire field program when $z/L < -0.1$.

5. Vertical structure

The buoyancy-generation of turbulence energy is quite small compared to the shear-generation and dissipation (Figure 2), although this weak buoyancy flux strongly influences the vertical structure, as discussed

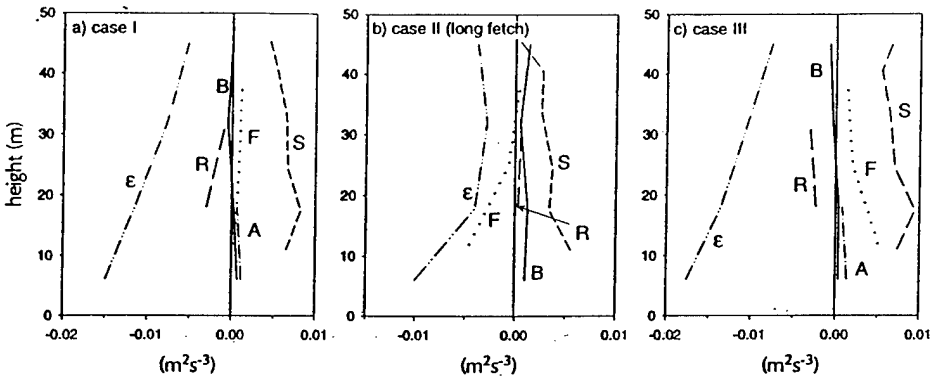

Figure 2. The turbulence energy budget (m^2s^{-3}) for the weakly unstable cases. A is the advection term, ϵ the dissipation, S the shear-generation term, F the vertical divergence of the flux of the turbulence energy and B the buoyancy-generation term. The residual, R, is computed from the two levels where all the terms can be evaluated.

Table I. Case Studies. B.F. is the surface buoyancy flux ($°Cms^{-1}$) averaged over the 3, 6 and 10 m levels, "travel" refers to the travel time in minutes, fetch is in kilometers and V is the 10 m wind speed. Case I for the stable and unstable flows include time-height cross-sections of the buoyancy flux (Figures 1 and 4).

case study	Time (DOY)	travel	fetch	B.F.	wind ms^{-1}	z/L
unstable-UI	291.9 - 293.0	5	3	0.02	10	-0.10
unstable-UII	289.25 - 290	35	18	0.03	9	-0.11
unstable-UIII	307.7 - 308.35	4.5	2.8	0.01	10	-0.02
stable-SI	297.0 - 297.7	5	2	-0.02	7	0.44
stable-SII	299.0 - 301.0	6	2.8	-0.01	8	0.06
stable-SIII	303.15 - 303.25	5	2	-0.01	6.5	0.11

below. For unstable conditions, the horizontal advection of turbulence energy is also small in the turbulence energy budget, at least near the surface where it could be evaluated (Figure 2a, c). Horizontal advection presumably becomes increasingly important at higher levels and also shoreward of the seamast.

For the two short fetch cases, the turbulent transport term the vertical flux convergence is positive near the surface (Figure 2), which

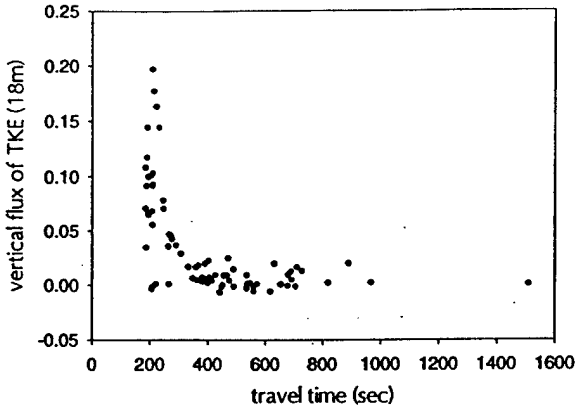

Figure 3. The dependence of the vertical flux of turbulence energy ($m^3 s^{-3}$) at 18 m on travel time for all of the one-hour records with fetch values less than 5 km for unstable conditions ($z/L < -0.1$).

would be consistent with the fact that the tower occupies the bulk of the internal boundary layer. For the long fetch case, the vertical flux divergence term is negative near the surface corresponding to traditional export of turbulence energy upward out of the surface layer.

In contrast to the short fetch cases, the flow in Case UII reaches the tower after a relatively long fetch of 18 km and travel time of about 35 min. The flow is unstable at all levels and the momentum flux for Case UII is approximately constant with height, within the uncertainty due to differences between different sonic anemometers. The unstable internal boundary layer is deep compared to the tower layer because of the longer travel time over the water. The buoyancy flux is small and erratic for this case due to small air-sea temperature difference and the flux shows no obvious trend with height.

The layer of upward buoyancy flux is capped by a layer of downward buoyancy, which sometimes is as thick as, or thicker than, the layer of upward buoyancy flux. This vertical structure is seen in the first part of Figure 2, after which the depth of the convective layer grows and engulfs the entire tower layer. In the former case, the vertically integrated buoyancy flux is small or even negative and the vertically-integrated turbulence is driven by shear-generation.

The turbulent transport of turbulence energy (Figure 3) is often large upward for unstable cases with short travel time of less than 300s where advection from land is most important. The turbulent transport is never significant downward. For stable offshore flow, the pattern is quite different (next section).

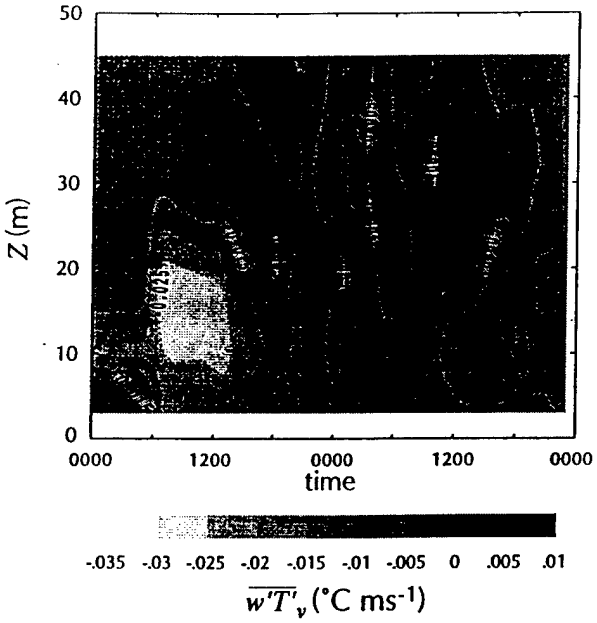

Figure 4. Time-height cross-section of the buoyancy flux ($°Cms^{-1}$) for stable case SI where lighter areas correspond to stronger downward buoyancy flux. Times are GMT which is one hour behind local solar time.

6. Downward buoyancy flux

Flow of warm air over a cooler surface is now analyzed in terms of three case study periods where the magnitude of the downward buoyancy flux at the surface is greater than 0.01 $°Cms^{-1}$ for most of the episode. The time-height cross-section for the buoyancy flux is shown for the case with the largest sustained downward buoyancy flux (Figure 4). For this case, the downward buoyancy flux at the sea surface is due to advection of warm air from the heated land surface over the cooler water and exhibits significant diurnal variation. The vertical structure of the turbulence kinetic energy budget is averaged for all of the one-hour records in each of the three cases (Figure 5 a-c). All three cases correspond to short fetch and short travel time (Table 1) and weak stability. We will also analyze statistics based on all of the individual one-hour records during the entire field program when $z/L > 0.1$.

6.1. Elevated stress maximum

For stable periods, the stress often increased with height (Vickers and Mahrt, 1999). This occurred for even weak stability but was more

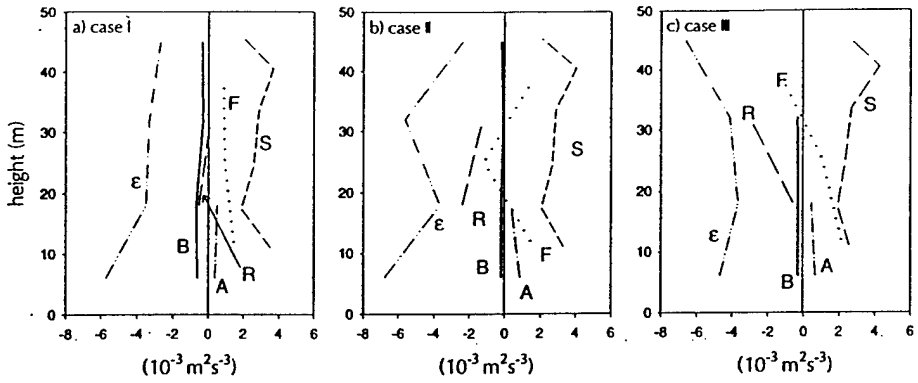

Figure 5. The turbulence energy budget ($10^{-3}m^2s^{-3}$) for the three weakly stable Cases (a-c). A is the advection term, ϵ the dissipation, S the shear- generation term, F the vertical divergence of the flux of the turbulence energy, B the buoyancy-generation term and R, the residual.

pronounced for the few cases of stronger stability, as in Figure 6, where the measured stress and downward heat flux near the surface have essentially collapsed, within measurement error. This vertical structure is quite different from observed traditional stable boundary layers where the stress, buoyancy flux and turbulence energy decrease monotonically with height (Caughey et al., 1979; Lenschow et al., 1987; Sorbjan, 1988). In the present observations of offshore flow, the elevated maxima of stress and turbulence energy are maintained by shear-generation and presumably augmented by advection of stronger turbulence from land.

The stress convergence below the elevated stress maximum acts to accelerate the flow and may account for much of the observed flow acceleration downstream from the coast. The observed vertical convergence of stress at the sea mast, applied over the travel time from the coast, corresponds to an acceleration of 0.5-1.0 ms^{-1}. The observed acceleration ranged from 0.8 - 1.3 ms^{-1}. A rigorous assessment of the momentum budget is prevented by inadequate assessment of the local horizontal pressure gradient.

The observed increase of stress with height does not appear to be related to instrumentation differences. For long-fetch, near-neutral conditions, the observed stress is essentially constant with height across the tower layer (or decreases very slowly with height), as expected in non-advective traditional boundary layers where the boundary layer is much deeper than the tower layer.

An elevated stress maximum is also observed by Glendening (personal communication) in an LES model of flow from a rough surface to a smooth surface with zero buoyancy flux. He used this elevated stress

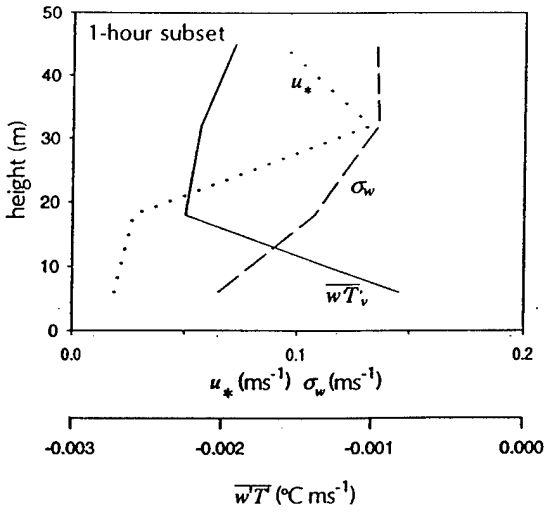

Figure 6. Vertical profiles of the friction velocity (ms^{-1}), buoyancy flux ($°Cms^{-1}$) and σ_w (ms^{-1}) for a one-hour period during case SI where surface fluxes are very weak.

maximum to define the top of the new internal boundary layer. The elevated maximum was maintained by horizontal advection. Definition of the top of the internal boundary layer in terms of a stress maximum contrasts sharply with definition of the top of the internal boundary layer in terms of a minimum of turbulence, cited in the Introduction. The differences of the vertical structure may be due to different relative position downstream from the surface change. The present observations in offshore flow are short fetch and Mengelkamp (1991) finds that the minimum develops beyond a certain fetch offshore.

To form a simple measure of the vertical structure of the stress for individual records, the ratio of stress in the upper part of the tower layer to that in the lower part of the tower layer, is computed as:

$$stress\ ratio = \frac{stress_{upper}}{stress_{lower}} \tag{2}$$

where $stress_{upper}$ is the average of the stress magnitude at the two upper tower levels, 32 m and 45 m, and the $stress_{lower}$ is the average of the three lowest levels, 3 m, 6 m and 10 m. This ratio is computed for all of the one-hour records where $z/L > 0.1$. The momentum flux ratio is sometimes large for small travel time, exceeding two in a significant fraction of the cases (Figure 7). These values correspond to a rapid increase of stress with height. The momentum flux ratio decreases rapidly with increasing travel time to values closer to unity for travel times of

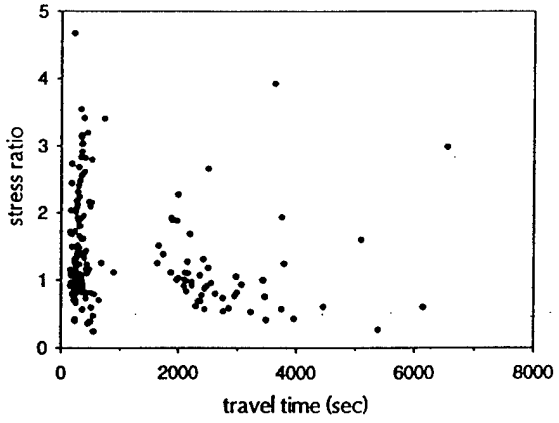

Figure 7. The stress ratio (Eq. 2) as a function of travel time for all of the one-hour records with stable conditions ($z/L > 0.1$).

ten minutes and longer, although the scatter is large. For values near unity, the stress changes slowly with height, implying that the internal boundary layer is deep compared to the tower layer.

What generates this vertical structure? Firstly, the shear-generation term tends to increase with height (Figure 5), in contrast to the usual boundary layer where it decreases rapidly with height. Secondly, the turbulence advected horizontally from land in offshore flow is thought to decay more slowly at higher levels where the turbulence length scale is larger. The dissipation rate divided by the turbulence energy decreases with height for both stable and unstable cases. Finally, the advection of stress might increase with height due to increasing wind speed with height.

6.2. Downward transport of turbulence

For Cases SI and SIII, the vertical turbulent transport of turbulence kinetic energy is significant downward (not shown), implying that the main source of turbulent kinetic energy is elevated and the near surface flow is a sink of turbulence energy. This downward transport of turbulence energy is consistent with the increase of turbulence and stress with height. The downward transport of turbulence kinetic energy leads to significant vertical flux convergence of turbulence energy at the lower levels (Figure 5). The turbulence near the surface is therefore partly maintained by downward transport of turbulence energy. The downward transport of turbulence toward the surface may be augmented by

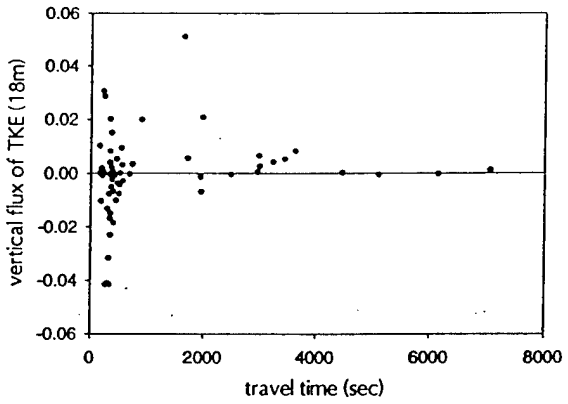

Figure 8. The dependence of the vertical flux of turbulence energy ($m^3 s^{-3}$) at 18 m on travel time for all of the one-hour records with stable conditions ($z/L > 0.1$).

the pressure transport term in the turbulence kinetic energy equation (Smedman et al., 1995).

Considering all of the stable one-hour records, the vertical transport of turbulence energy for short travel times is often large positive (Figure 8), as also occurred in the unstable offshore flow cases. However, in contrast to unstable conditions, the vertical transport of turbulence energy is sometimes large downward for short travel times less than 300 s (Figure 8), again implying that the main source of turbulence is elevated in some stable offshore flows. These cases of downward transport of turbulence energy normally correspond to an increase of stress with height (Figure 9, momentum flux ratio > 1). Our attempts to model this type of "boundary layer" have not been successful to date.

7. Conclusions

For the present data, weakly convective internal boundary layers in flow of cooler air over warmer water are sometimes capped by a relatively thick layer of downward buoyancy flux. In such cases, the vertically integrated buoyancy flux is small or even negative and the vertically-integrated turbulence is driven by shear-generation and possibly horizontal advection.

With advection of warm air over cooler water, the vertical structure may be quite different even though the flow is normally only weakly stable ($z/L < 0.5$). These cases often occur in the afternoon with flow

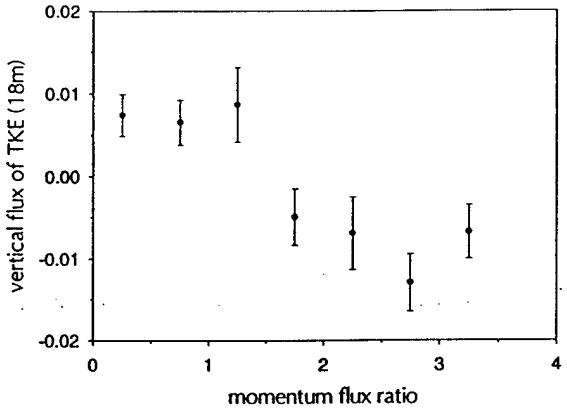

Figure 9. The relationship between the turbulence energy flux ($m^3 s^{-3}$) at 18 m and the momentum flux ratio for stable conditions based on bin-averaged values computed from the one-hour records. Also shown are standard error bars.

of warm air from the heated land surface. In some cases, the turbulence energy and stress increase with height, reaching an elevated maximum, and the transport of turbulence energy is sometimes downward toward the surface, in contrast to unstable conditions. This structure was observed with travel times less than 10 minutes (fetches generally less than 5 km). The increase of stress with height appears to be maintained by horizontal advection of stronger turbulence from land and shear-generation associated with accelerating flow over the water.

The downward transport of turbulence kinetic energy over the sea implies that the net generation of turbulence over the water surface is much weaker than over the upstream land surface due to a combination of stability and reduced surface roughness over the sea. These two effects are not separable in that stable stratification restricts the downward transport of momentum to the sea surface, which leads to very small surface roughness lengths. Consequently, the overall effect of buoyancy is greater than that over land where the roughness length is essentially constant. The relationship between the roughness length and the stability may contribute to the large differences in vertical structure of the flow for the cases of weak upward and weak downward buoyancy flux, which occur even though the buoyancy term in the turbulence kinetic energy equation is small compared to shear-production and dissipation.

Acknowledgements

We gratefully acknowledge the important comments of Peter Taylor and an anonymous reviewer and the computational assistance of Sesha Sadagopan. This material is based upon work supported by Grant N0001409810282 from the Office of Naval Research, Marine Meteorology.

References

Barthelmie, R. J., Courtney, M. S., Højstrup, J., and Sanderhoff, P.: 1994, 'The Vindeby Project: A Description', Report R-741(EN), Risø National Laboratory, DK4000, Roskilde, Denmark.

Barthelmie, R. J., Grisogono, B., and Pryor, S. C.: 1996, 'Observations and Simulations of Diurnal Cycles of Near-Surface Wind Speeds over Land and Sea', *J. Geophys. Res.* **101**, 21,327-21,337.

Caughey, S. J., Wyngaard, J. C., and Kaimal, J. C.: 1979, 'Turbulence in the Evolving Stable Boundary Layer', *J. Atmos. Sci.* **36**, 1041-1052.

Edson, J. and Fairall, C. W.: 1998, 'Similarity Relationships in the Marine Atmospheric Surface Layer for Terms in the TKE and Scalar Variance Budgets', *J. Atmos. Sci.* **55**, 2311-2328.

Garratt, J. R.: 1987, 'The Stably Stratified Internal Boundary Layer for Steady and Diurnally Varying Offshore Flow', *Boundary-Layer Meteorol.* **38**, 369-394.

Garratt, J. R.: 1990, 'The Internal Boundary Layer - a Review', *Boundary-Layer Meteorol.* **50**, 171-203.

Garratt, J. R. and Ryan, B. F.: 1989, 'The Structure of the Stably Stratified Internal Boundary Layer in Offshore Flow over the Sea', *Boundary-Layer Meteorol.* **47**, 17 - 40.

Hare, J. E., Hara, T., Edson, J. B., and Wilczak, J. M.: 1997, 'A Similarity Analysis of the Structure of Airflow over Surface Waves', *J. Phy. Oceanog.* **27**, 1018-1037.

Højstrup, J., Edson, J., Hare, J., Courtney, M. S., and Sanderhoff, P.: 1997, 'The RASEX 1994 Experiments', Risø -R-788, Risø National Laboratory, Roskilde, Denmark, (ISBN-87-550-2039-9), 24 pp.

Lenschow, D. H., Li, X. S., Zhu, C. J., and Stankov, B. B.: 1987, 'The Stably Stratified Boundary Layer over the Great Plains. I. Mean and Turbulence Structure', *Boundary-Layer Meteorol.* **42**, 95-121.

Mahrt, L., Vickers, D., Howell, J., Højstrup, J., Wilczak, J. A., Edson, J., and Hare, J.: 1996, 'Sea Surface Drag Coefficients in RASEX', *J. Geophys. Res.* **101**, 14327-14335.

Mengelkamp, H.-T.: 1991, 'Boundary Layer Structure over an Inhomogeneous Surface: Simulation with a Non-Hydrostatic Mesoscale Model', *Boundary-Layer Meteorol.* **57**, 323-342.

Nieuwstadt, F. and Brost, R.: 1986, 'The Decay of Convective Turbulence', *J. Atmos. Sci.* **43**,532-546.

Plant, W., Keller, W. Hesany, V. and Hayes, K.: 1998: 'Measurements of the Marine Boundary Layer from an Airship', *J. Atmos. Oceanic. Tech.* **15**, 1433-1458.

Smedman, A.-S., Bergström, H., and Högström, U.: 1995,'Spectra, Variances and Length Scales in a Marine Stable Boundary Layer Dominated by a Low Level Jet', *Boundary-Layer Meteorol.* **76**, 211-232.

Smedman, A.-S., Bergström, H., and Grisogano, B.: 1997, 'Evolution of Stable Internal Boundary Layers Over a Cold Sea', *J. Geophys. Res.* **102**, 1091-1099.

Sorbjan, Z.: 1988, 'Structure of the Stably-Stratified Boundary Layer During the SESAME-1979 Experiment', *Boundary-Layer Meteorol.* **44**, 255-266.

Sorbjan, Z.: 1997, 'Decay of Convective Turbulence Revisited', *Boundary-Layer Meteorol.* **82**, 501-515.

Sun, J., Desjardins, R., Mahrt, L., and MacPherson, J. I.: 1998, 'Transport of Carbon Dioxide, Water Vapor and Ozone by Turbulence and Local Circulations', *J. Geophys. Res.*, **103**, 25,873-25,885.

Sun, J., Vandemark, D., Mahrt, L., Vickers, D., Crawford, T., Vogel, C., and Dumas, E.: 2000, 'Momentum Transfer over the Coastal Zone', Submitted to *J. Geophys. Res.*.

Tjernström, M. and Smedman, A.-S.: 1993, 'The Vertical Structure of the Coastal Marine Atmospheric Boundary Layer', *J. Geophys. Res.* **98**, 4809-4826.

Vickers, D. and Mahrt, L.: 1999, 'Observations of Nondimensional Shear in the Coastal Zone', *Quart. J. Roy. Met. Soc.*, **125**, 2685-2702.

Wilczak, J., Edson, J., Højstrup, J., and Hara, T.: 1999, 'The Budget of Turbulent Kinetic Energy in the Marine Atmospheric Surface Layer', *Air-Sea Exchange - Physics, Chemistry, Dynamics and Statistics*, G. Geernaert, editor, Kluwer.

Air-Sea Exchange: Physics, Chemistry and Dynamics

Edited by

G.L. GEERNAERT

National Environmental Research Institute,
Roskilde, Denmark

KLUWER ACADEMIC PUBLISHERS
DORDRECHT / BOSTON / LONDON

A C.I.P. Catalogue record for this book is available from the Library of Congress.

ISBN 0-7923-5937-2

Published by Kluwer Academic Publishers,
P.O. Box 17, 3300 AA Dordrecht, The Netherlands.

Sold and distributed in North, Central and South America
by Kluwer Academic Publishers,
101 Philip Drive, Norwell, MA 02061, U.S.A.

In all other countries, sold and distributed
by Kluwer Academic Publishers,
P.O. Box 322, 3300 AH Dordrecht, The Netherlands.

Printed on acid-free paper

Printed in the Netherlands.

Chapter 10

THE COASTAL ZONE

LARRY MAHRT
College of Oceanic and Atmospheric Sciences
Oregon State University
Corvallis, OR 97331, USA

10.1 Introduction

The coastal zone is of considerable practical importance since it is a region of intensive human activity and rich in biological activity, compared to the open ocean. At the same time, the spatial variation of the atmospheric surface flow and the surface wave field are complex and both are often in nonequilbrium. Formulations of surface stress must include the influence of developing wave state and shoaling (Section 3). Growing waves occur with offshore flow and with time-varying wind fields, often induced by diurnal variation of the heat flux discontinuity at the coastal interface (Section 5). Current formulations of the surface flux may perform poorly in developing internal boundary layers in offshore flow (Section 4). Difficulties with formulation of surface fluxes in the coastal zone is a major topic of this chapter (Sections 2-3). Offshore flow must adjust to smaller surface roughness and different surface heat flux over the sea. The modelling problem is particularly difficult with offshore flow of warm air over a cool water surface (Section 4). The development of stratus and other cloud regimes in the coastal zone is beyond the scope of this survey. This chapter will assume familiarity with previous reviews found in Donelan (1990) and Geernaert (1990).

10.2 Formulation of surface fluxes

The surface stress, heat flux and moisture flux are formulated through the bulk formulas:

$$(\overline{w'u'}^2 + \overline{w'v'}^2)^{1/2} = C_d \overline{u}^2 \qquad (10\text{-}1)$$

G.L. Geernaert (ed.), Air-Sea Exchange: Physics, Chemistry and Dynamics, 247–267.

$$\overline{w'\theta'} = C_h\overline{u}[\theta_o - \overline{\theta}] \qquad (10\text{-}2)$$

$$\overline{w'q'} = C_q\overline{u}[q_o - \overline{q}] \qquad (10\text{-}3)$$

where C_d is the drag coefficient, C_h is the transfer coefficient for heat, C_q is the transfer coefficient for moisture, z is the observational height, θ_o and q_o are surface aerodynamic values of the potential temperature and specific humidity, to be defined below, and $\overline{u}$ is the speed of the vector averaged wind where the x-coordinate has been rotated into the direction of the mean wind. Similar bulk formulations can be written for turbulent transfer of other scalars although definition of the aerodynamic surface quantities becomes problematic (Sun et al. 1998a). Numerous variations of the bulk formula are used where the vector averaged speed is replaced by the averaged instantaneous speed, the total stress is replaced by the stress in the along-wind direction, or the current velocity is removed from the wind (see Mahrt et al. 1998). Since the stress, wind and wave propagation directions may be systematically different (Geernaert 1990; Rieder et al. 1994; Rieder 1996), omission of the cross wind stress seems inadvisable even though this component can be characterized by large flux sampling errors.

In the case of weak winds, the precise definition of the velocity used in the bulk formula becomes important. This velocity scale has been generalized to include the influence of "large convective eddies" (Beljaars 1995; Fairall et al. 1996; Grachev et al. 1998) or mesoscale motions which are on smaller scales than the spatial or grid-averaging scale (Mahrt, Sun 1995; Vickers, Esbensen 1998). Resolving this problem is made difficult by severe flux sampling errors in the weak wind case (Mahrt et al. 1996) which can be reduced only with long stationary records. With weak winds and swell, the momentum flux may even be transported from the waves to the atmosphere (e.g. Smedman et al. 1994).

The simplest formulation of the surface stress specifies the neutral drag coefficient to be constant or a function of wind speed but independent of wave state (see studies surveyed in Geernaert, 1990). The transfer coefficient for heat is often specified to be constant where θ_o is equated to the surface radiation surface temperature of the water or the near-surface water temperature and q_o is specified to be the saturation specific humidity evaluated at the value of the surface temperature. The appealing simplicity of this approach meets the demand of economy required in some large scale models.

However, in the coastal zone, stability strongly influences the transfer coefficients. One might expect stability $-z/L$ to be smaller over water than over land since surface heat fluxes are typically smaller over water than over land, where L is the Obukhov length

$$L \equiv \frac{u_*^3}{\kappa z (g/\theta_v)\overline{w'\theta_v'}} \qquad (10\text{-}4)$$

where u_* is the surface friction velocity (square root of the surface stress magnitude) and κ is the von Karman constant. However, the shear stress is also weaker over the sea than over land due to small surface roughness so that the stability $-z/L$ can significantly influence the transfer coefficients even without strong surface buoyancy flux. As a

result, stability may strongly influence the flux-gradient relationship in the coastal zone. To include the influence of stability on the drag coefficient and transfer coefficients, Monin-Obukhov similarity theory (Monin, Obukhov 1954) is applied by either:

1) using similarity theory to reduce the drag and transfer coefficients to their equivalent neutral values (Section 10.2.2) and relating the neutral values to the wind speed and wave state or
2) explicitly applying Monin-Obukhov similarity theory and relating the roughness length to wave state (Section 10.3.2).

10.2.1 MONIN-OBUKHOV SIMILARITY THEORY

Monin-Obukhov similarity theory provides a model for the flux-gradient relationship in the surface layer, above the wave boundary layer (Figure 10.1). In the surface layer, the flux-gradient relationship is assumed to be independent of the wave state and a universal function of only z/L. This flux-gradient relationship is posed in terms of the nondimensional vertical gradient

$$(z/L) \equiv \frac{(\partial\overline{\theta}/\partial z)(\kappa z\, u_*)}{\overline{w'\theta'}(z)} \qquad (10\text{-}5)$$

$$\phi_m(z/L) \equiv \frac{(\partial\overline{u}/\partial z)(\kappa z)}{u_*} \qquad (10\text{-}6)$$

which have been empirically fitted to dependencies on z/L (Högström 1988). The nondimensional gradient ϕ can be interpreted as the inverse of the mixing efficiency. The transfer of moisture and other scalars are often assumed to follow the same dependence as that for heat. This interpretive survey will concentrate on transfer of heat and momentum as examples.

The surface drag coefficient and transfer coefficient for heat are estimated by vertically integrating the ϕ functions downward to the surface roughness lengths in which case one can derive:

$$C_d = \left[\frac{\kappa}{ln(z/z_o) - \psi_m}\right]^2 \qquad (10\text{-}7)$$

$$C_h = \left[\frac{\kappa}{ln(z/z_o) - \psi_m}\right]\left[\frac{\kappa}{ln(z/z_{oh}) - \psi_h}\right] \qquad (10\text{-}8)$$

where z_o and z_{oh} are the roughness lengths for momentum and heat, respectively, and ψ and ψ_h are the integrated analytical forms of the nondimensional gradients for momentum and heat, ϕ_m (z/L) and ϕ_h (z/L). This vertical integration (Paulson, 1970) requires that the fluxes and the wind direction are approximately independent of height and requires additional mathematical approximations (Enriquez, Friehe 1997). The nondimensional vertical gradients, ϕ_m (z/L) and ϕ_h (z/L), have not been extensively evaluated over the sea. Recently, Højstrup (1998) found that for onshore flow in the coastal zone, the land-based stability dependence for ϕ_m (z/L) approximated the observed

values of ϕ_m although the scatter was large. Conflicting evidence is noted in the next subsection.

Note that Monin-Obukhov similarity theory does not describe the actual flux-gradient relationship below the surface layer in the wave boundary layer. The extrapolated wind profile described by similarity theory vanishes at the roughness height z_o instead of at the surface. As a result, the extrapolated and actual wind profiles in the wave boundary layer are not expected to be the same. The extrapolated profile of potential temperature is also expected to be different from the actual profile in the wave boundary layer, and reaches the "aerodynamic" surface temperature at the roughness height for heat, z_{oh}. Both the aerodynamic surface temperature θ_o and z_{oh} are unknown. Specifying θ_o to be the surface radiation temperature or near-surface water temperature redefines the roughness height for heat z_{oh}. Over the open ocean, the thermal roughness height is normally related to the roughness length for momentum (Lui et al. 1979). In the coastal zone, Mahrt et al. (1998) find little relationship between z_{oh} and z_o where z_{oh} appears to be strongly influenced by development of internal boundary layers while z_o is more influenced by wave state. Both the physical meaning of the roughness height for heat and its dependence on other parameters remain elusive, especially in the coastal zone.

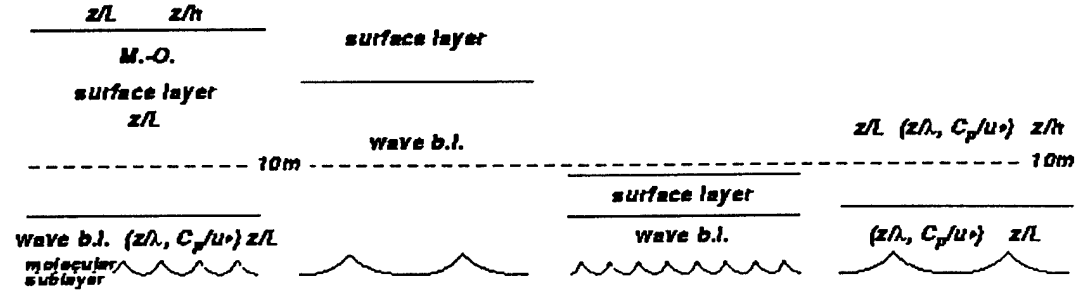

Figure 10.1 Idealized layering of the lower boundary layer. Using 10 m as a reference height, the first scenario shows the ideal case where Monin-Obukhov similarity theory applies. In the second example, the reference level is in the wave boundary layer and wave length scales are required to describe the local flux-gradient relationship. In the third example, the reference level is above the surface layer and bulk boundary-layer scaling is required. In the fourth example, the influence of the boundary-layer depth extends downward to the wave boundary layer and the conditions for Monin-Obukhov similarity theory are not met at any level.

10.2.2 REDUCING TO NEUTRAL

To eliminate the influence of stability, the drag coefficient and transfer coefficients are sometimes reduced to their neutral values (Deardorff 1968). This procedure attempts to eliminate the influence of stability so that the neutral drag and transfer coefficients can be studied as a function of wave state and wind speed. The reduction of the transfer coefficient to neutral conditions using Monin-Obukhov similarity theory must impose restrictions on the roughness length such as Charnock's relationship with constant coefficient (Geernaert, Katsaros 1986; Geernaert 1990). Smith (1980, Figure 13),

Geernaert (1988) and Mahrt et al. (1996) find that the reduction of the drag coefficient to neutral values does not completely remove the influence of stability although it is not clear if the stability functions $\phi_m(z/L)$ and $\phi_h(z/L)$ themselves are incorrect, measurement errors are large or influences not included in the Obukhov length are large.

10.2.3 WAVE BOUNDARY LAYER

The wave boundary layer is the layer adjacent to the wave surface, but above the very thin laminar sublayer at the surface (Figure 10.1). In the wave boundary layer, part of the atmospheric transporting motions are directly induced by the waves and associated perturbation pressure field in the air (Chalikov, Belevich 1993; Hare et al. 1997). The depth of the wave boundary layer is thought to scale with the surface wavelength (Chalikov, Belevich 1993). Multiple wave boundary layers associated with wind driven waves and swell may coexist. However, the transport by eddies in phase with the swell may be small since the swell are characterized by small slopes. In the wave boundary layer, Monin-Obukhov similarity theory does not describe the local flux-gradient relationship which depends partly on the amplitude and wavelength of the dominant surface wave (Large et al. 1995). Apparently, the profile functions, ϕ_m and ϕ_h depend on z/λ as well as z/L (or equivalently z/L and λ/L) where λ is a dominant wave dimension, either wave length or wave height.

Consequently, Monin-Obukhov similarity theory must be applied in the surface layer above the wave boundary layer, along with specified roughness lengths, in order to predict the surface fluxes. Analogously, over land, Monin-Obukhov similarity must be applied in the surface layer above the roughness sublayer to predict surface fluxes. Eqs. (10-1)-(10-2) correctly predict surfaces fluxes using Monin-Obukhov similarity theory for the drag and transfer coefficients (Eqs. (10-7)-(10-8)) only if the roughness lengths can be appropriately specified.

There are two fundamental differences between the flux-gradient relationship over the sea and that over land:

1) In the roughness sublayer over land, the time-averaged flow may vary horizontally on the scale of the roughness elements due to semi-stationary pressure perturbations anchored to individual roughness elements. Over the sea, the roughness elements (surface waves) propagate so that such microscale spatial variability of the time-averaged flow does not normally exist.
2) Over the sea, the roughness length for momentum varies substantially with wave state. Over land, z_o is normally considered to be independent of time for a given wind direction.

However, there is no obvious reason why these differences would reduce the applicability of Monin-Obukhov similarity theory over the sea, provided that the appropriate surface roughness lengths can be specified in a reasonably simple fashion. In fact, Monin-Obukhov similarity theory is more likely less applicable over land where the required assumption of homogeneity is normally violated to some degree. Even over apparently homogeneous land surfaces, microscale variations of soil moisture can influence local eddy structure. Nonetheless, there are special processes in the coastal zone which violate assumptions required for Monin-Obukhov similarity theory.

10.2.4 THEORY BREAKDOWN IN THE COASTAL ZONE

Existing similarity theory may break down in the coastal zone due to the following influences:

1. Strong horizontal advection leads to significant vertical divergence of the flux. For example with steady-state temperature advection, $\overline{u}\partial\overline{\theta}/\partial x \approx -\partial\overline{w'\theta'}/\partial z$. Then the assumption of height-independent fluxes is not a good approximation and the vertical integration of the nondimensional gradients, ϕ, to obtain the stability corrections for the transfer coefficients, ψ (Eqs. (10-7)-(10-8)), is not valid.
2. If the flux decreases to small values at the top of the thin internal boundary layers in offshore flow, then the vertical divergence of the flux is large. As a result, standard observational levels, such as 10 m, may be above the thin surface layer where one can neglect the height-dependence of the flux (Figure 10.1). The depth of the surface layer is bounded by some small fraction of the boundary-layer depth, sometimes chosen as 10%, such that the height-dependence of the flux can be neglected in the surface layer. For example, in an internal boundary layer of 50 m depth, the surface layer would theoretically be less than 5 m depth. Note that influences 1) and 2) are not independent.
3. With offshore flow of warm air over cold water, the turbulence may be a top-down process where the primary source of turbulence is above the surface inversion (Section 10.4.2). It is not clear if Monin-Obukhov similarity theory is valid in this "upside-down boundary layer".
4. The turbulence in offshore flow does not establish equilibrium with the rapidly evolving mean flow immediately downstream from the coast.
5. With cold (warm) air advection in offshore flow, the wind vector tends to rotate to the right (left) with height and the surface stress vector is directed to the right (left) of the surface wind vector (Geernaert 1988). Integration of Monin-Obukhov similarity theory assumes that the wind and stress vectors are aligned and their height-dependence can be neglected.
6. It may be that Monin-Obukhov similarity theory is valid but the stability functions, ϕ_m and ϕ_h, are not correctly calibrated.

If the internal boundary layer is sufficiently thin, yet the wave boundary layer is deep (large surface wavelength), the surface layer may be "squeezed out" as postulated by Mahrt et al. (1998) and shown in Figure 10.1 (right hand side). That is, there is no layer where the flux-gradient relationship depends only on z/L and the influence of boundary-layer depth, h, and surface wave dimension λ must be included as additional scaling variables. Grant (1992) suggests that $\phi(z/L)$ for the near neutral boundary layer should be generalized to be of the form $\phi(z/h,\ h/L,\ u_*/fh)$ where f is the Coriolis parameter. Khanna and Brasseur (1997) consider the form $\phi(z/L,\ h/L)$. In the LES results of Khanna and Brasseur (1997), the nondimensional shear decreases above the surface layer, as is also observed by Smedman and Johannson (1997) in shallow offshore boundary layers. With a well-mixed interior of the boundary layer, the vertical gradient decreases faster with height than the flux. Mahrt et al. (1998) find that the thin depth of observed offshore internal boundary layers suppresses heat transfer by the large convective eddies which in turn implies that ϕ_h is larger than predicted by Monin-Obukhov similarity theory and depends on z/h.

Davidson (1974) found that ψ_m and the drag coefficient are both a function of stability and wave age and that these dependencies are difficult to sort out since the wave age and stability were significantly correlated for their data. Bergström and Smedman (1995) examined the functional dependence ϕ_m (z/L, C_p/u_*) but found that the relationship to wave state was statistically insignificant, although they note that their data represents a relatively narrow range of conditions. Here, C_p is the phase speed of the dominant wave.

Since for offshore flow, there may be no level where ϕ_m is a function of only z/L, it is useful to consider a more general formulation such as

$$\phi_m \equiv \frac{(\partial \overline{u}/\partial z)\ (\kappa z)}{u_*} = f(z/L,\ z/\lambda,\ C_p/u_*, z/h) \qquad (10\text{-}9)$$

Note that the arguments z/L, z/λ, C_p/u_*, z/h are not independent. Large et al. (1995) prefer to partition the nondimensional shear into two functions, the traditional ϕ_m (z/L) and a modifying function $\chi(z/\lambda)$, as also pursued by Vickers and Mahrt (1998). Specific forms of Eq. (10-9) based on actual eddy correlation data have not been established.

Monin-Obukhov similarity theory is also complicated by the possible dependence of the von Karmen "constant" on the roughness Reynolds number, Re_* defined as $u_* z_o/\nu$. Generally, $\kappa(Re^*)$ is found to decrease with increasing roughness Reynolds number (Tennekes, 1968). With this possibility, evaluation of $\phi_m(z/L)$ from data using Eq. (10-6) results in two unknowns, $\kappa(Re_*)$ and $\phi_m(z/L)$. Oncley et al. (1996), Miller et al. (1997) and others eliminate $\phi_m(z/L)$ as an unknown by considering near neutral cases and assuming $\phi_m(z/L) = 1$. Then, $\kappa(Re_*)$ is estimated as

$$\kappa(Re_*) = \frac{u_*}{z\partial \overline{u}/\partial z} \qquad (10\text{-}10)$$

Since both Re_* and z/L depend on u_*, their dependencies are difficult to isolate from data. For example, failure to include the dependence $\kappa(Re_*)$, if important, would alter the value of $\phi_m(z/L)$ computed from data. Conversely, if influences of z/L are not completely negligible, such influences could create an artificial dependence of κ on the roughness Reynolds number. The problem becomes even more complex if the nondimensional shear is dependent on wave age (Eq. (10-9) since the wave age also depends on u_*.

10.3 Wave state

In the coastal zone, the stress is influenced by shoaling processes and wave breaking as waves propagate into shallow water (Smith 1980; Freilich et al. 1990). For waves propagating toward the shore, wave modification first occurs when the depth of the water shallows to be about 1/4 of the dominate wavelength. At this point, the wave amplitude begins to increase, the wavelength and propagation speed begin to decrease and the spectral characteristics change. Closer to the shore where the depth becomes less than one wave height, dramatic wave steepening and breaking occur (Thornton,

Guza 1982, 1983; Holman, Sallenger 1985; Holland et al. 1995). Irregularities of the bottom topography along the coast and wave refraction lead to irregularities in the surface wave field along the coast (Munk, Traylor 1947).

Information on wave state is necessary for modelling surface stress in the coastal zone. This information is included at three levels of approximation: 1) relating the drag coefficient or roughness length to the wave age is the most common approach (Section 10.3.1), 2) relating the stress to different frequency bands of the wave field, such as swell and wind-driven modes, is more complete but requires more information on the wave field (Section 10.3.2) and 3) modelling the wave age in terms of fetch is less accurate but is useful when explicit information on wave state is not available (Section 10.3.3).

10.3.1 WAVE AGE DEPENDENCE

With offshore flow, the wind driven waves are growing in the downstream direction which become evident seaward of the inner shoaling zone. A number of investigators have documented that the stress is greater over a young and developing wave field than over an older wave field, which is in near-equilibrium with the wind field (e.g. Donelan 1990; Kitaigorodskii 1973; Nordeng 1991; Geernaert et al. 1987, 1988; Donelan 1990; Maat et al 1991). At least two mechanisms contribute to the dependence of stress on wave age: 1) younger waves propagate with slower phase speed relative to the wind and thus provide greater bulk shear, and 2) younger growing waves may be steeper, which can lead to enhanced flow separation from individual wave crests. Younger developing waves occur with changing wind vector as well as with fetch limited off-shore flow.

Previous studies suggest that the drag coefficient is a maximum for a wave age of 10 (Nordeng 1991) and 7 (Geernaert, Smith 1996). Kitaigorodskii et al. (1995) similarly find maximum roughness length at an intermediate wave age. In the absence of swell (inland seas), the drag coefficient may be immeasurably small immediately downstream from the shore where waves have not yet developed or are very small amplitude. The subsequent wave growth in the downstream direction leads to larger stress, as sketched in Figure 10.2. The wave growth in the downwind direction can be further enhanced by acceleration of the offshore wind resulting from the smaller surface roughness over the sea than over land. However, at some point, the increasing phase speed of the waves and resulting reduction of the relative flow of the wind over the waves becomes more important than the effect of increasing wave amplitude and any increase of slope. Then the stress and drag coefficient begin to decrease further downstream. Consequently, the drag coefficient reaches a maximum at an intermediate wave age and decreases with further increase of wave age. Similar effects appear in the model of Hansen and Larsen (1997) where the Charnock constant reaches a maximum at a wave age of about 5. Most observations occur at wave ages greater than this intermediate wave age so that the drag coefficient is generally considered to decrease with increasing wave age, as in the studies surveyed below.

Vickers and Mahrt (1997) find that onshore flow with shoaling, can also occur with small values of the wave age. The shoaling reduces the wave phase speed and decreases the numerical value of the wave age. Consequently, shoaling complicates the physical interpretation of wave age in the coastal zone. The corresponding drag coefficient may increase by more than 50% with such shoaling. As a result, Kitaigorodskii et al. (1995) related the momentum roughness length to wave breaking characteristics. Mahrt et al. (1998) found no detectable increase in the transfer coefficients for heat and moisture

with wave breaking. Relative insensitivity of the transfer coefficients for heat and moisture to wave state and wind speed was also found in Smith (1980), Makin and Mastenbroek (1996) and references therein.

Since the stress appears to be related to the relative flow of the air with respect to the phase speed of the dominate waves (Kitaigorodskii 1973), one is tempted to re-define the drag coefficient in terms of the relative flow $\bar{u} - C_p$ where C_p is ideally the component of the phase speed of the dominant wave in the wind direction. However, the stress does not necessarily vanish as $\bar{u} - C_p$ approaches zero, since waves with frequencies different from the dominant wave contribute to the stress and propagate with different phase velocities. For example, with mature waves, much of the stress is thought to be associated with capillary waves and therefore not related to the phase speed of the dominant waves. As a result of the stress from capillary waves, the alternate drag coefficient, defined as the ratio of the stress to $\bar{u} - C_p$, approaches infinity as $\bar{u} - C_p$ approaches zero.

However the traditional drag coefficient computed from (Eq. (10.1)) may be better related to $\bar{u} - C_p$ than $\bar{u}$ alone. To examine this problem, we computed the drag coefficient from eddy correlation data collected at a tower 2 km off the Danish coast in the Risø Air Sea Experiment (RASEX, Barthelmie 1994; Højstrup et al. 1994; Mahrt et al. 1996). The drag coefficient reaches a minimum value near $\bar{u} - C_p = 0$ m/s and a regression model of the drag coefficient based on $\bar{u} - C_p$ explains more variance than that based on $\bar{u}$. However, the drag coefficient is more closely related to wave age than $\bar{u} - C_p$ probably because wave age implicitly accounts for the relative flow over the waves as well as implicitly includes the effect of wave amplitude and steepness.

Geernaert et al. (1987) proposed a model of the dependence of the neutral drag coefficient on wave age of the form

$$C_{dn} = b\,(C_p/u_*)^{-2/3} \qquad (10\text{-}11)$$

where b is on the order of 10^{-2}. Vickers and Mahrt (1997) found that this model performed well in the coastal zone even after accounting for the role of self-correlation. They found that -2/3 was indeed the best fit to the exponent while the best fit value of b was approximately 7×10^{-3}.

The drag coefficient can also be computed directly from Monin-Obukhov similarity theory in which case the roughness length is a function of wave state. The Charnock (1955) prediction of the roughness length, $0.019\,(u_*^2/g)$, is often generalized to include a dependence on inverse wave age (Toba, Koga 1986; Maat et al. 1991; Donelan 1990; Smith et al. 1992). If we also incorporate the smooth flow contribution to the roughness length (Donelan 1990; Fairall et al. 1996), then the full relationship is of the form

$$z_o = K\,(u_*^2/g)\,(u_*/C_p)^p + 0.11\,\nu/u_* \qquad (10\text{-}12)$$

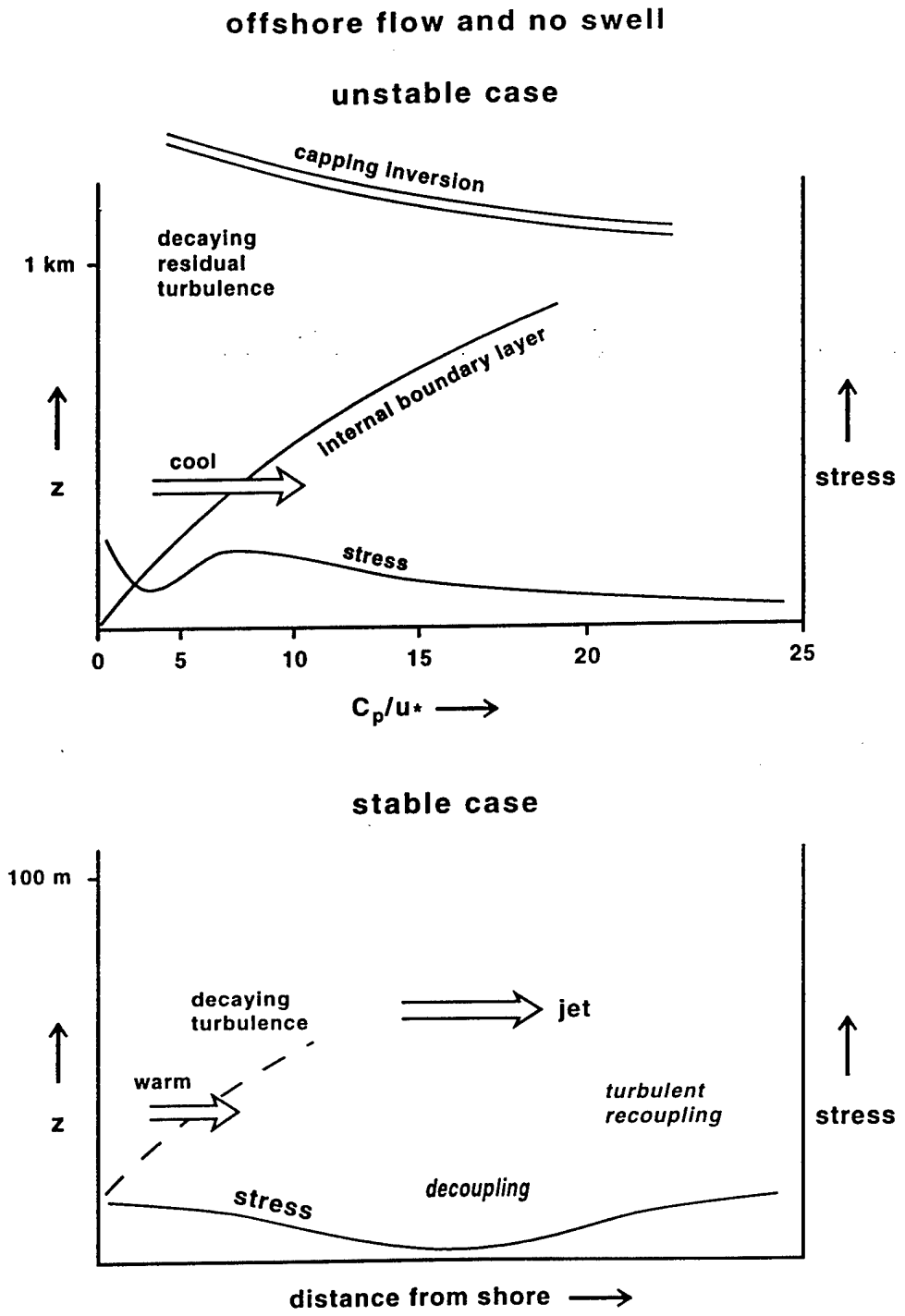

Figure 10.2 Plausible schematic evolution of the internal boundary layer for unstable and very stable offshore flows. In the unstable case, the x-axis can also be qualitatively interpreted as the downstream distance.

where typically K=0.48 and p=1 (Smith et al. 1992), and ν is the viscosity of air. Wu (1968) suggested an additional term due to parameterized surface tension which was recently applied in Alam and Curry (1997).

Alternatively, the model of Kitaigorodskii (1970) is of the form,

$$z_o = K\sigma\exp(-\kappa C_p/u_*) \qquad (10\text{-}13)$$

where $K = 0.3$, σ is the root mean square amplitude of the waves and κ is von Karman's constant. The Kitaigorodskii representation follows from explicitly including the shear between the wind and the wave velocity and integrating over the full wave spectrum.

A significant fraction of the variance explained by these models is due to self-correlation since the drag coefficient and roughness length are both defined in terms of the surface friction velocity and are both formulated in terms of the surface friction velocity on the right hand sides of Eqs. (10-11)-(10-13) (e.g. Smith et al. 1992; Vickers, Mahrt 1997). To avoid self-correlation, the wave age is sometimes expressed in terms of $C_p/\overline{u}$ where $\overline{u}$ is the wind speed at a standard level or at a fixed height relative to the surface wavelength (Donelan 1990).

The roughness length is sometimes related to other characteristics of the wave field. For example, Anctil and Donelan (1996) relate the spatial variation of the roughness length in the shoaling zone to the wave age, root mean squared displacement height of the waves and root mean square wave slope. Kitaigorodskii et al. (1995) relate the roughness length to the effective wave height.

10.3.2 MULTI-MODE MODELS

The need for models based on multiple wave modes is motivated by the fact that the wind driven waves and swell often propagate in different directions. The swell modifies the stress direction so that it may be different from the wind direction (Geernaert et al. 1995). A family of parameterizations of the roughness length as a weighted integral of the wave spectra have been formed from the original framework of Kitaigorodskii (1973) as in Hansen and Larsen (1997). See also Chalikov and Belevich (1993) and papers surveyed in Geernaert (1990). Kitaigorodskii et al. (1995) focus on the width of the wave dissipation regime in an effort to understand the variability of surface roughness. The most complete description of the wave field can be obtained from explicit wave models such as the "WAM" model (WAMDI group, 1988). The advantage of relating the surface roughness to the wave spectra avoids the parameterized coupling between the surface roughness and with the wind field or stress field itself that occurs with the approaches in the preceding section. At the same time, complete information on the full wave spectra is normally not available.

Simplified models which allow some information of differences between wave modes include the two band model of Donelan (1982) which distinguishes between the drag associated with short and long waves. Vickers and Mahrt (1997) develop a crude indicator of the wave state based on that band width of the spectra which accounts for 50% of the wave energy. Narrow band spectra are associated with near-equilibrium single mode waves and smaller drag coefficient while broad band spectra are more associated with multi-peaked spectra, confused seas and/or non-equilibrium wave state, all leading to larger drag coefficients.

10.3.3 FETCH DEPENDENT MODELS

For many applications, the wave phase speed and wave age are not known. As an alternative simpler approach, the inverse wave age can be parameterized in terms of either F_*, based on the friction velocity (Perrie, Toulany 1990, Geernaert, Smith 1996), or F_u, based on the 10 m wind speed. These parameterizations are of the form:

$$u_*/C_p = w_o + \frac{\alpha}{F_*} \tag{10-14}$$

$$u_*/C_p = w_o + \frac{\alpha}{F_u} \tag{10-15}$$

where based on dimensional arguments:

$$F_* \equiv \left(\frac{gX}{u_*^2}\right)^{1/3} \tag{10-16}$$

$$F_u \equiv \left(\frac{gX}{U^2}\right)^{1/3} \tag{10-17}$$

Here X is the upwind fetch distance and w_o and α are determined empirically. Eq. (10-14) explains more variance than Eq. (10-15) but is characterized by self-correlation. Vickers and Mahrt (1997) find that Eq. (10-15) is a reasonable approximation for offshore flow in the coastal zone flow, although errors are larger compared to formulations based on wave state information.

Direct relationship of the roughness length to the fetch can be found in Geernaert (1988b). More complete models first describe the dependence of the wave field on fetch and then link the drag to the fetch-dependent wave field (Geernaert 1990).

10.4 Internal boundary layers

With any wind component perpendicular to the coast, internal boundary layers form due to the temperature and surface roughness contrast between the water and land surfaces. The internal boundary layer is the layer of air adjacent to the surface which is influenced by the new surface (e.g. Garratt 1990).

10.4.1 UNSTABLE CASE

With offshore flow of cold air over warmer water, a convectively driven internal boundary layer forms in response to the upward buoyancy flux over the water. This layer thickens in the downstream direction (Figure 10.2). These internal boundary layers are sometimes found to be well defined by a sharp change of properties between the convectively driven turbulence and fluid, at least in terms of instantaneous observations (Raynor et al. 1979; Sun et al. 1998b). It is not known if such sharply defined tops of the internal boundary layer are normal nor is it known if the internal boundary layer top for time-averaged flow is thick due to vacillation of the boundary-layer top.

Figure 10.3 shows the averaged vertical structure for a nine-hour period of stationary offshore advection of cold air observed in RASEX (Section 10.3.1). Several features occur in Figure 10.3 which are not typical of the "textbook" unstable internal boundary layer:

1) For the averaged flow, the "entrainment zone" with downward heat flux is thicker than the convective layer of upward buoyancy flux.
2) The total buoyancy-destruction of turbulence in the entrainment zone is greater than the buoyancy-generation of turbulence in the surface-based convective layer. Therefore, turbulence near the top of the internal boundary layer must be maintained by local shear-generation, as observed in Sun et al. (1998b).
3) The turbulence and stress are a maximum near the *top* of the convective layer.
4) The mean shear increases with height corresponding to convex curvature. This curvature implies inflection points near the surface and somewhere above the 45 m tower layer.

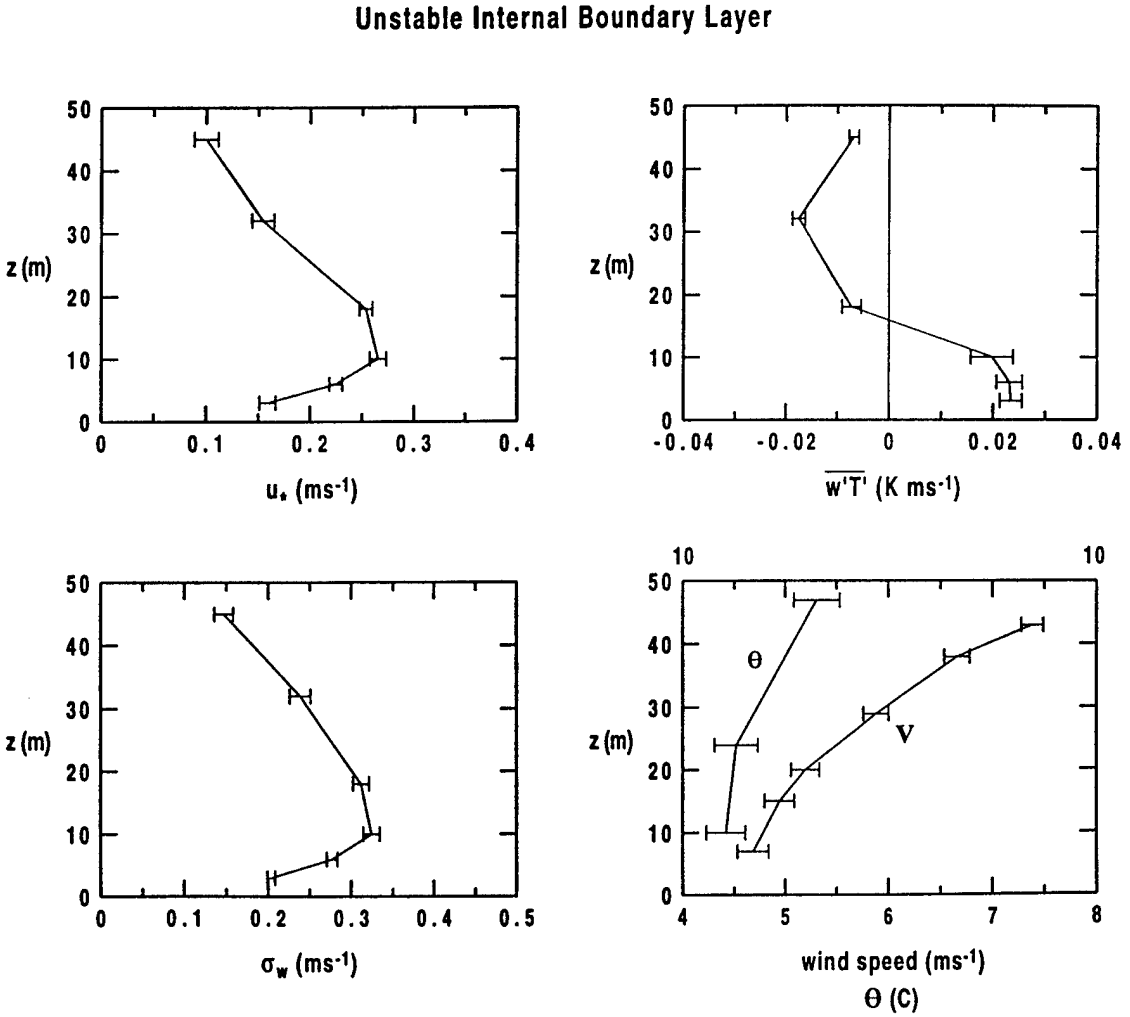

Figure 10.3 The 5-hour averaged vertical structure of relative stationary offshore flow of cool air over warmer water observed in RASEX. Fluxes are based on perturbations from a 10-minute simple mean.

Is this structure unique to these data or does the traditional concept of internal boundary layers not apply immediately downstream from the coast? The RASEX data set is the first data set with detailed vertical resolution of the time-averaged structure in offshore flow.

Källstrand and Smedman (1997) compare various models of growth of the internal boundary layer against aircraft data collected in a developing internal boundary layer over land with onshore flow. Although most of the models have been developed for the unstable internal boundary layer over land (e.g., Melas, Kambezidis 1992; Gryning, Batchevarova 1990), they should in principal apply over the sea in the coastal zone. The internal boundary layer is traditionally modelled on two separate scales (Garratt 1990): small scales on the order of a kilometer or less and the mesoscale on a horizontal scale of tens of kilometers or more. On the scale of a kilometer or less, the heated internal boundary layer entrains upward through the old boundary layer (Vugts, Businger 1977). On this scale, the initial growth rate of the convective internal boundary layer is thought to be linearly proportional to the strength of the turbulence in the convective internal boundary layer such that (Høstrup 1981; Brutsaert 1982; Garratt 1990)

$$\frac{dh_{IBL}}{dx} = C\frac{\sigma_w}{U} \qquad (10\text{-}18)$$

where h_{IBL} is the depth of the internal boundary layer and σ_w is the standard deviation of the turbulent fluctuations of vertical velocity, often parameterized in terms of the surface friction velocity and the convective velocity scale. The wind speed U is evaluated at the top of the internal boundary layer. Since stratification of the overlying fluid is neglected, no additional velocity scales are included. The value of C is thought to be order of unity (Mahrt 1996).

Some investigators have formulated analytical expressions for the small scale growth of the internal boundary-layer depth. For example, Andreas et al. (1979, 1981) model the depth in terms of the fetch. Observations of such internal boundary-layer growth are summarized in Andreas and Cash (1998).

Further downstream, on the mesoscale, the convective internal boundary layer completes its growth through the old boundary layer (Figure 10.2) and begins entraining nonturbulent fluid, as occurs in flow of cold air over warm water studied in Chang and Braham (1991), Smith and MacPherson (1987), Rogers et. al. (1995) and Brümmer (1996). A well-defined capping inversion usually develops and information on the stratification of the overlying fluid is required to predict further growth of the convective internal boundary layer. Models for this case are surveyed in Garratt (1990) and Källstrand and Smedman (1997).

10.4.2 STABLE CASE

The growth of the stable internal boundary layer due to flow of warm air over cooler water is expected to be slower because of buoyancy destruction of turbulence associated with the downward heat flux. For example, based on temperature profiles in Gryning (1985), the growth rate dh_{IBL}/dx in the stable internal boundary layer in the coastal zone is less than 1%. A thick residual layer of decaying turbulence extends from the top of the thin stable internal boundary layer to the top of the advected continental boundary

layer (Rogers et al. 1995). The growth of the internal boundary layer for stable conditions is also described by Mulhearn (1981) and Garratt (1990).

The vertical structure of the stable internal boundary layer may be well defined in offshore flow (e.g. Garratt, Ryan 1989) where turbulence quantities monotonically decrease with height. However, if the water temperature is much cooler than the advected air, the turbulence at the surface may collapse resulting in decoupling of the overlying advected turbulence from the surface (Figure 10.2). Such collapse cannot be predicted with existing similarity theory which is the basis for surface fluxes in numerical models. Above the surface inversion over the water, the advected turbulence from land decays in the downstream distance. Since the change of surface heat flux, viewed by a moving Lagrangian column, is almost instantaneous as it crosses the land-sea boundary, the forcing time scale due to the change of surface flux is small compared to the internal time scale of the turbulence (turbulent length scale/turbulent velocity scale). Then the turbulence decays in a self-similar fashion leading to a square root dependence on time (Sorbjan 1997).

In addition to the decaying turbulence above the surface inversion, elevated shear-generation of turbulence is observed further downstream. The flow above the surface inversion, which was part of the boundary layer over land, accelerates and forms a low level jet (Smedman et al. 1995), analogous to formation of a low-level jet above the nocturnal surface inversion (Figure 10.2). Further downstream, the shear on the underside of the jet eventually generates turbulence and re-establishes a surface-based boundary layer. Still further downstream, the flow may become near neutral as the air finally cools to the value of the sea surface temperature (Smedman et al. 1997).

The RASEX data for offshore flow of warm air over cooler water (Figure 10.4) also indicate that the classical concept of an internal boundary layer does not apply. The stress, heat and turbulence energy are smaller near the surface and reach maximum values at higher levels in the tower layer. Note that the strength of the turbulence for the stable case is comparable to that for the unstable case (Figure 10.3) because the wind speeds for the stable case are larger. For shorter periods, the stress and turbulence in the stable case may temporarily collapse near the surface in that the stress is zero within measurement error. Then the elevated turbulence is semi-detached from the surface corresponding to an upside-down boundary layer.

10.4.3 ROUGHNESS CHANGE

Internal boundary layers may also form due to spatial variation of the surface roughness between the land, shoaling zone and open ocean. With offshore flow, the smaller roughness over the sea compared to over the land leads to flow acceleration and decreased turbulence strength in the downstream direction, as observed in Smith and MacPherson (1987). Although the roughness increases in the downstream direction (Figure 10.2), it remains much smaller than the roughness over land.

Normally, at least some surface temperature discontinuity occurs at the coast so that internal boundary layers result as combination of surface roughness and surface heat flux changes. For example, Barthelmie et al. (1996) find that in unstable boundary layers associated with flow of cool nocturnal air over warmer water, winds accelerate due to smaller roughness over the water. However with stable internal boundary layers associated with daytime flow of warmer air over the water, the reduction of downward

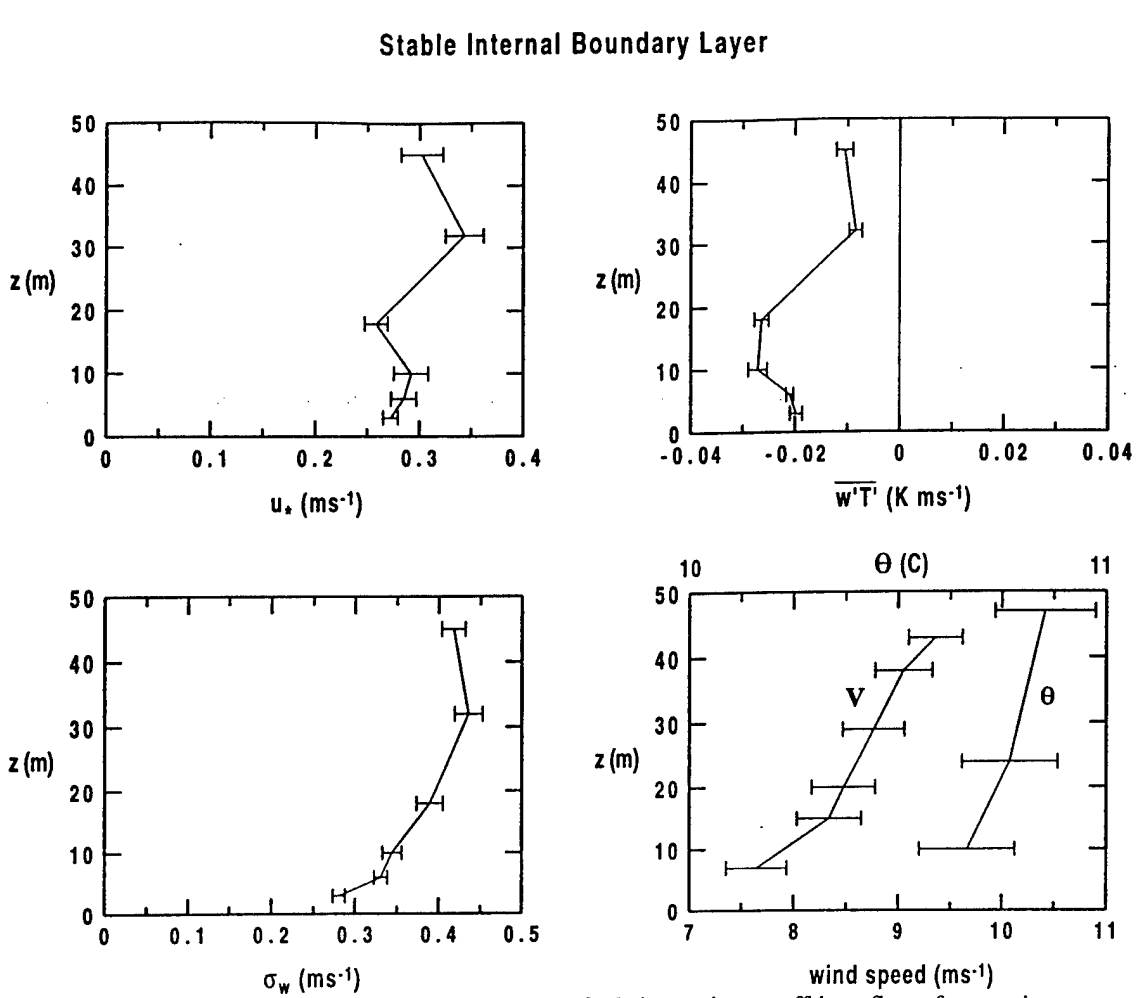

Figure 10.4 The 9-hour averaged vertical structure of relative stationary offshore flow of warm air over cooler water observed in RASEX. Fluxes are based on perturbations from a 10 minute simple mean.

mixing of momentum due to stable stratification counteracts the effect of decreased surface roughness on the wind speed. As a result, acceleration over the water was not normally observed in the daytime.

10.5 Local circulations

10.5.1 SEA/LAND BREEZES

The land-sea interface not only leads to development of internal boundary layers but also modifies the low level pressure field through differential surface heating. On sunny days, surface heat flux from the heated land surface warms the atmosphere and lowers the surface hydrostatic pressure over the land. Simultaneous heating does not occur over the water surface since: a) the heat capacity of the water is large, b) the solar radiation is absorbed over the first few meters instead of at the surface, as occurs over land, and c) heat from absorbed solar radiation is mixed downward by oceanic turbulence which is much more efficient than thermal conduction in the soil. As a result, a horizontal pressure gradient force develops directed toward the land surface. In the absence of significant opposing horizontal pressure gradient on the synoptic scale, the local

horizontal pressure gradient drives flow inland over the heated land surface, referred to as the sea breeze (Pielke 1984; Simpson 1994).

At night, surface cooling and associated downward heat flux cools the atmosphere leading to higher atmospheric pressure over the land surface. The resulting horizontal pressure gradient drives the land breeze over the sea. The nocturnal land breeze is thinner and weaker than the daytime sea breeze and is easily prevented by significant synoptic scale flow. The land breeze is rapidly eliminated by convective mixing as it flows over the warmer water (Sun et al. 1998b).

10.5.2 COASTAL TERRAIN SLOPES

Most coasts are characterized by sloping land surface. These slopes exert two independent influences on local circulations: 1) modification of the pressure field through surface heating on the sloped terrain and 2) pressure adjustments associated with topographically forced vertical motions in a stratified atmosphere. With sunny conditions, surface heating over the sloped land surface causes upslope flow in the daytime and downslope at night which augments the sea/land breeze circulation system. The slope flows may be non-hydrostatic for steep small scale slopes and approximately hydrostatic for larger scale weak slopes (Mahrt 1982).

Rising motion forced by onshore flow and sloped terrain corresponds to adiabatic cooling in the stratified atmosphere which in turn increases the underlying hydrostatic pressure. Much of this pressure increase can be associated with thickening of a cool surface marine layer capped by an inversion. The resulting local pressure gradient acts to reduce onshore flow. As a result, onshore flow decelerates before reaching the coast and the local winds at the coast are mainly parallel to the shore with rising terrain at the coast. The parallel flow may assume the form of a low level jet (Zemba, Friehe 1987).

Even flow approximately parallel to the coast experiences mesoscale disturbances induced by irregularities of the coastline. Circulations include supercritical flow (Winant et al. 1988; Samelson, Lentz 1994), coastal-trapped disturbances (Holland, Leslie 1986; Samelson, Rogerson 1996; Mass, Albright 1987), gravity currents (Dorman 1987) and a variety of other mesoscale flows (Beardsley et al. 1987). These mesoscale perturbations may be modulated by diurnal variations associated with differential surface heating, discussed above. In addition, atmospheric and oceanic circulations are coupled in the coastal zone. As one example, Zembe and Friehe (1987) examine the influence of wind acceleration and increased stress, resulting upwelling and reduction of surface temperature. The resulting increased atmospheric stability acts to reduce the stress.

10.6 Conclusions

Airflow in the coastal zone is complex due to formation of internal boundary layers, diurnally varying horizontal pressure gradients and strong spatial variation of the wave field. Assumptions required by Monin-Obukhov similarity theory may not be met due to surface heterogeneity, advection and strong vertical divergence of the flux. The surface airflow is not only coupled to the spatially varying wave field but also coupled to oceanic circulations through the sea surface temperature. Complex topography at the coast further complicate the total flow system. The above interpretive survey did not include a number of important topics such coastal zone cloud systems and special effects of bottom bathymetry. Improved understanding of fluxes in the coastal zone

must begin with observations of spatial variation of the flux with simple bathymetry, straight coast line and no significant topography.

10.7 Acknowledgments

The scientific comments and computational assistance of Dean Vickers and the suggestions of Jielun Sun, Rob Holman and Roger Samelson are greatly appreciated. This material is based upon work supported by grant N00014-1-98-1-0282 from the Office of Naval Research.

10.8 References

Alam, A.,. Curry, J.A. (1997) Determination of surface turbulent fluxes over leads in Arctic sea ice. *J. Geophys. Res./*, **102**, 3331-3334.

Anctil, F., Donelan, M.A. (1996) Air-water momentum flux observations over shoaling waves. *J. Phy. Oc.*, **26**, 1344-1353.

Andreas, E. L., Murphy, B. (1979) Velocity spectra and cospectra and integral statistics over Arctic leads. *Q. J. R. Meteorol. Soc.* **105** 1053-1070.

Andreas, E. L., Williams, R. M., Paulson, C. A. (1981) Observations of condensate profiles over Arctic leads with a hot-film anemometer. *Q. J. R. Meteorol. Soc.* **107** 437-460.

Andreas, E. L., Cash, B.A. (1998) Convective heat transfer over wintertime leads and polynyas. submitted to *Quart. J. Roy. Met. Soc./*.

Beardsley, R.C., Dorman, C:E., Friehe, C.A., Rosenfeld, L.K., Winant, C.D. (!987) Local atmospheric forcing during the coastal ocean dynamics experiment. 1. A description of the marine boundary layer and atmospheric conditions over a northern California upwelling region. *J. Geophys. Res.* **92** 1467-1488.

Barthelmie, R. J., Courtney, M.S., Højstrup, J., Sanderhoff, P. (1994) The Vindeby Project: A Description. Report R-741(EN), Risø National Laboratory, DK4000, Roskilde, Denmark.

Barthelmie, R. J., Grisogono, B., Pryor, S.C. (1996) Observations and simulations of diurnal cycles of near-surface wind speeds over land and sea. *J. Geophys. Res.* **101** 21,327-21,337.

Beljaars, A.C. (1995) The parameterization of surface fluxes in large scale models under free convection. *Quart. J. Roy. Met. Soc.*, **121**, 255-270.

Bergström, H., Smedman, A. (1995) Stably stratified flow in the marine surface layer. *Boundary-Layer Meteorol./*, **72**, 239-265.

Brutsaert, W. H. (1982) *Evaporation into the Atmosphere*. D. Reidel, Dordrecht, 299 pp.

Brümmer, B. (1996) Boundary-layer modification in wintertime cold-air outbreaks from the Arctic sea ice. *Boundary-Layer Meteorol./*, **80**, 109-125.

Chalikov, D. V., Belevich, M.Y. (1993) 'One-Dimensional Theory of the Wave Boundary Layer'. *Boundary-Layer Meteorol./*, **63**, 65-96.

Chang, S. S., Braham, R.R., Jr. (1991) Observational study of a convective internal boundary layer over Lake Michigan. *J. Atmos. Sci./*, **48**, 2265-2279.

Charnock, H. (1955) `Wind stress over a water surface', *Quart. J. Roy. Met. Soc./*, **81**, 639-640

Davidson, K. L. (1974) Observational results on the influence of stability and wind-wave coupling on momentum transfer and turbulent fluctuations over ocean waves. *Boundary-Layer Meteorol./*, **6**, 303-323.

Deardorff, J. W. (1968) Dependence of Air-Sea Transfer Coefficients on Bulk Stability. *J. Geophys. Res.*, **73**, 2549-2557.

Donelan, M. (1982) The dependence of the aerodynamic drag coefficient on wave parameters. *First International Conference on Meteorology and Air-Sea Interaction of the Coastal Zone*, Amer. Met. Soc., 381-387, 1982.

Donelan, M. (1990) Air-sea interaction, in *Ocean Engineering Science*, edited by B. Le Mehaute, and D. M. Hanes, 239-291, John Wiley and Sons.

Dorman, C.E. (1987) Possible role of gravity current in northern California's coastal summer wind reversals. *J. Geophys. Res.*, **92**, 1497-1506.

Enriquez, A. G., Friehe, C.A. (1997) Bulk parameterization of momentum, heat, and moisture fluxes over a coastal upwelling area. to appear in *J. Geophys. Res./*.

Freilich, M. H. R., Guza, R.T., Elgar, S.L. (1990) Observations of nonlinear effects in directional spectra of shoaling gravity waves, *J. Geophys. Res./*, **95**, 9645-9656.

Garratt, J. R. (1990) The internal boundary layer - a review. *Boundary-Layer Meteorol./*, **50**, 171-203.

Garratt, J. R., Ryan, R.F. (1989) The structure of the stably stratified internal boundary layer in offshore flow over the sea. *Boundary-Layer Meteorol./*, **47**, 17-40.

Geernaert, G.L (1988a) Influence of coastal fetch-limited waves on determining the wind stress during diabatic conditions. *Ninth Symposium on Turbulence and Diffusion*, Roskilde, Denmark, Amer. Met. Soc. 54-57.

Geernaert, G.L (1988b) Drag coefficient modelling for the near-coastal zone. *Dyn. Atmos. Oceans*, **11**, 307-322.

Geernaert, G. L.(1990) Bulk parameterizations for the wind stress and heat fluxes. *Surface Waves and Fluxes. Vol. 1 - Current Theory*, 91-172, G. L. Geernaert and W. J. Plant, Eds., Kluwer.

Geernaert, G.L., Katsaros, K.B. (1986) Incorporation of stratification effects on the oceanic roughness length in the derivation of the neutral drag coefficient, *J. Phy. Oc.*, **16**, 1580-1584.

Geernaert, G. L., Larsen, S.E., Hansen, F. (1987) Measurements of the wind stress, heat flux and turbulence intensity during storm conditions over the North Sea, *J. Geophys. Res./*, **92**, 13,127-13,139.

Geernaert, G. L., Davidson, K.L., Larsen, S.E., Mikkelsen, T. (1988) Wind stress measurements during the Tower Ocean Wave and Radar Dependence Experiment, *J. Geophys. Res./*, **93**, 13,913-13,923.

Geernaert, G.L., Smith, J.A. (1998) `On the fetch dependent drag coefficient over coastal and inland seas', NERI Report 227, National Environmental Research Institute, Roskilde, Denmark, 10 pp.

Grachev, A. A., Fairall, C. W., Larsen, S. I. (1998) On the determination of the neutral drag coefficient in the convective boundary layer. *Boundary-Layer Meteorol./*, **86**, 423-439.

Grant, A. L. M. (1992) The structure of turbulence in the near-neutral atmospheric boundary layer. *J. Atmos. Sci./*, **49**, 226-239.

Garratt, J. R. (1990) The internal boundary layer - a review. *Boundary-Layer Meteorol./*, **50**, 171-203.

Gryning, S.-E. (1985) The Øresund Experiment - A nordic mesoscale dispersion experiment over a land-water-land area. *Bull. Amer. Meteor. Soc./*, **66**, 1403-1407.

Gryning, S.-E., Batchvarova, E. (1990) Analytical model for the growth of the coastal internal boundary layer during onshore flow. *Quart. J. Roy. Met. Soc./*, **78**, 405-413.

Hansen, C., Larsen, S.E. (1997): Further work on the Kitaigorodskii roughness length model: A new derivation using Lettau's expression for steep waves. *Geophysica*, **33**, 29-44.

Hare, J. E., Hara, T., Edson, J.B., Wilczak, J.M. (1997) A similarity analysis of the structure of airflow over surface waves. *J. Phy. Oc.*, **27**, 1018-1037.

Högström, U. (1988) Non-dimensional wind and temperature profiles in the atmospheric surface layer: A re-evaluation. *Boundary-Layer Meteorol./*, **42**, 55-78.

Højstrup, J. (1981) A simple model for the adjustment of velocity spectra in unstable conditions downstream of an abrupt change in roughness and heat flux. *Boundary-Layer Meteorol./*, **21**, 341-356.

Højstrup, J. (1998) Stability effects on offshore wind profiles. submitted to *Boundary-Layer Meteorol./*.

Højstrup, J., Edson, J., Hare, J., Courtney, M.S., Sanderhoff, P. (1997) The RASEX 1994 experiments, *Risø -R-788, (ISBN-87-550-2039-9)*, 24 pp, Risø National Laboratory, Roskilde, Denmark.

Holman, R. A., Sallenger, A.H., Jr. (1985) Setup and swash on a natural beach. *J. Geophys. Res./*, **90**, 945-953.

Holland, G.J., Leslie, L.M. (1986) Ducted coastal ridging over S.E. Australia. *Q. J. R. Meteorol. Soc.*, **112**, 731-748.

Holland, K. T., Raubenheimer, B., Guza, R.T. (1982) Runup kinematics on a natural beach. *J. Geophys. Res./*, **100**, 4985-4993.

Källstrand, B., Smedman, A-S. (1997) A case study of the near-neutral coastal internal boundary-layer growth: Aircraft measurements compared with different model estimates. *Boundary-Layer Meteorol./*, **85**, 1-33.

Khanna, S., Brasseur, J.G. (1997) Analysis of Monin-Obukhov similarity from large eddy simulation. *J. Fluid Mech.*, **345**, 251-286.

Kitaigorodskii, S.A. (1973) `The physics of air-sea interaction', translated from Russian, Israel Program for Scientific Translations, Jerusalem, 273 pp.

Kitaigorodskii, S.A., Volkov, Y.A., Grachev, A.A. (1995) A note on the analogy between momentum transfer across a rough solid surface and the air-sea interface. *Boundary-Layer Meteorol./*, **76**, 181-197.

Kroon, L.M.M., De Bruin, H A R. (1993) Atmosphere-vegetation interaction in local advective conditions: effect of lower boundary conditions. *Agric. For. Meteorol. /*, **64**, 1-28.

Large, W. G., Morzel, J., Crawford, G.B. (1995) Accounting for surface wave distortion of the marine wind profile in low-level ocean storms wind measurements. *J. Phy. Oc.*, **25**, 2959-2971.

Liu, W. T., Katsaros, K.B., Businger, J.A., Tillman, J.E. (1979) Heat transport and thermal structure in the interfacial boundary layer measured in an open track of water in turbulent free convection. *J. Atmos. Sci.*, **36**, 1722-1735.

Maat, N., Kraan, C., Oost, W.A. (1991) The roughness of wind waves, *Boundary-Layer Meteorol./*, **54**, 89-103, 1991.

Mahrt, L. (1982) Momentum balance of gravity flows. *J. Atmos. Sci.*, **39**, 2701-2711.

Mahrt, L. (1996) The bulk aerodynamic formulation over heterogeneous surfaces, *Boundary-Layer Meteorol./*, **78**, 87-119.

Mahrt, L., Sun, J. (1995) The subgrid velocity scale in the bulk aerodynamic relationship for spatially averaged scalar fluxes. *Mon. Wea. Rev./*, **123**, 3032-3041.

Mahrt, L., Vickers, D., Howell, J., Edson, J., Hare, J., Højstrup, J., Wilczak, J. (1996) Sea surface drag coefficients in RASEX. *J. Geo. Res., Oceans*, **101**, 14,327-14,335.

Mahrt, L., Vickers, D., Edson, J., Sun, J., Højstrup, J., Hare, J., Wilczak, J. (1998) Heat flux in the coastal zone. to appear in *Boundary-Layer Meteorol./*.

Makin, V. K., Mastenbroek, C. (1996) Impact of waves on air-sea exchange of sensible heat and momentum. *Boundary-Layer Meteorol./*, **79**, 279-300.

Mass, C.F., Albright, M.D. (1987) Coastal southerlies and along shore surges of the west coast of North America: Evidence of mesoscale topographically response to synoptic forcing. *Mon. Weather Rev.*, **115**, 1707-1738.

Melas, D., Kambezdis, H.D. (1992) The depth of the internal boundary layer over an urban area under sea-breeze conditions. *Boundary-Layer Meteorol./*, **61**, 247-264.

Miller, S., Friehe, C., Hristov, T., Edson, J. (1997) Wind and Turbulence Profiles in the Surface Layer over the Ocean. *12th Symposium on Boundary Layers and Turbulence*. Amer. Met. Soc., Vancouver, 273-274

Monin, A. S., Obukhov, A.M. (1954) Basic laws of turbulent mixing in the ground layer of the atmosphere. *Trudy Geofiz. Inst. Akad. Nauk SSSR*, **151**, 163-187.

Mulhearn, P.J. (1981) On the formation of a stably stratified inertial boundary layer by advection of warm air over a cooler sea. *Boundary-Layer Meteorol./*, **21**, 247-254.

Munk, W. H., Traylor, M.A. (1947) Refraction of ocean waves: A process linking underwater topography to beach erosion. *J. of Geology*, **55**, 1-26. [ITEM][] Nordeng, T. E., On the wave age dependent drag coefficient and roughness length at sea, *J. Geophys. Res./*, bf 96, 7167-7174, 1991.

Oncley, S. P., Friehe, C.A., LaRue, J.C., Businger, J.A., Itsweire, E.C., Chang, S.S. (1996) Surface-layer fluxes, profiles, and turbulence measurements over uniform terrain under near-neutral conditions. *J. Atmos. Sci./*, **53**, 1029-1044.

Paulson, C. A. (1970) The mathematical representation of wind speed and temperature profiles in the unstable atmospheric surface layer. *J. Appl. Meteor./*, **9**, 857-861.

Perrie, W., Toulany, B. (1990) `Fetch relations for wind-generated waves as a function of wind-stress scaling', *J. Phy. Oc.*, **20**, 1666-1681.

Pielke, R. A. (1984) *Mesoscale Meteorological Modeling*, Academic Press. New York, 612 pp.

Raynor, G S., Sethuraman, S., Brown, R:M. (1979) Formation and characteristics of coastal internal boundary layers during onshore flows. *Boundary-Layer Meteorol./*, **16**, 487-514.

Rieder, K. F., Smith, J.A., Weller, R.A. (1994) Observed directional characteristics of the wind, wind stress and surface waves on the open ocean, *J. Geophys. Res./*, **22**, 22,589-22,596.

Rieder, K.F. (1997) `Analysis of sea surface drag parameterizations in open ocean conditions', *Boundary-Layer Meteorol./*, **82**, 355-377.

Rogers, D., Rogers, P., Johnson, D.W., Friehe, C.A. (1995) The stable internal boundary layer over a coastal sea. Part I: Airborne measurements of the mean and turbulent structure. *J. Atmos. Sci./*, **52**, 667-683.

Samelson, R. M., Lentz S.J. (1994) The horizontal momentum balance in the marine atmospheric boundary layer during CODE-2. *J. Atmos. Sci./*. **51**, 3745-3757.

Samelson, R. M., Rogerson, A.M. (1996) Life-cycle of a linear coastal-trapped disturbance. *Mon. Wea. Rev.*, **124**, 1853-1863.

Simpson, J. E. (1994) *Sea Breeze and Local Winds*, Cambridge University Press, 234 pp.

Smedman, A.S., Tjernström, M., Högström, U. (1994) `Near-neutral marine atmospheric boundary layer with no surface shearing stress: A case study', *J. Atmos. Sci./*, **23**, 3399-3411.

Smedman, A-S, Bergström, H., Grisogano, B. (1997) Evolution of stable internal boundary layers over a cold sea. *J. Geophys. Res./*, **102**, 1091-1099.

Smedman, A-S., Johansson, C. (1997) Modifications of Monin-Obukhov similarity theory in unstable conditions. *12th Symposium on Boundary Layers and Turbulence*. Amer. Met. Soc., Vancouver, 273-274.

Smith, S.D. (1980) Wind stress and heat flux over the ocean in gale force winds, *J. Phy. Oc.*, **10**, 709-726.

Smith, S.D., Anderson, R.J., Oost, W.A., Kraan, C., Maat, N., DeCosmo, J., Katsaros,K.B., Davidson,K.L., Bumke,K., Hasse,L., Chadwick,H.M. (1992) `Sea surface wind stress and drag coefficients: the HEXOS results', *Boundary-Layer Meteorol./*, **60**, 109-142.

Smith, P.C., MacPherson, J.I. (1987) Cross-shore variations of near-surface wind velocity and atmospheric turbulence at the land-sea boundary during CASP. *Atmos-Ocean*, **25**, 279-303.

Sorbjan, Z. (YEAR!!!!)Decay of convective turbulence revisited. *Boundary-Layer Meteorol./*, **82**, 501-515.

Sun, J., Massman, W., Grantz, D.A., (1998a) Aerodynamic variables in the bulk formulation of turbulent fluxes. submitted to *Boundary-Layer Meteorol./*.

Sun, J., Desjardins, R., Mahrt, L., MacPherson, J.I. (1998b) Transport of carbon dioxide, water vapor and ozone by turbulence and local circulations. to appear in *J. Geophys. Res./*.

Tennekes, H. (1968) Outline of a second-order theory of turbulent pine flow. *AIAA*, **6**, 1735-1740.

Thornton, E.B. (1982) Energy saturation and phase speeds measured on a natural beach. *J. Geophys. Res./*, **87**, 9499-9508.

Thornton, E. B, Guza, R.T. (1983) Transformation of wave height distribution. *J. Geophys. Res./*, **88**, 5925-5938.

Toba,Y., Koga, M. (1986) `A parameter describing overall conditions of wave breaking, white capping, sea-spray production and wind stress', Oceanic Whitecaps D. Reidel, E. C. Monahan and G. Mac Niocaill Eds., 37-47.

Vickers, D., Mahrt, L. (1997) Fetch limited drag coefficients over shallow water. *Boundary-Layer Meteorol./*, **89**, 53-79.

Vickers, D., Esbensen, S.K. (1998) Subgrid surface fluxes in fair weather conditions during TOGA COARE: Observational estimates and parameterization. *Mon. Wea. Rev./*, **126**, 620-633.

Vickers, D., Mahrt, L. (1998) Nondimensional shear over surface waves. submitted to *Boundary-Layer Meteorol./*.

Vugts, H.F., Businger, J.A. (1977) Air modification due to a step change in surface temperature. *Boundary-Layer Meteorol./*, **11**, 295-306.

WAMDI group: Hasselmann, S., Hasselmann, K., Bauer, E., Janssen, P.A.E.M., Komen, G.J, Bertotti, L., Lionello, P., Guillaume, A., Cardone, V.C., Greenwood, J.A., Reistad, M., Zambresky, L., Ewing, J.A. (1988) The WAM model - A third generation ocean wave prediction model. *J. Phy. Oc.*, **18**, 1775-1810.

Wu, J. (1968) Laboratory studies of wind-wave interactions. *J. Fluid Mech.*, **68**, 49-70.

Zemba, J., Friehe, C.A. (1987) The marine atmospheric boundary layer jet in the coastal ocean dynamics experiment. *J. Geophys. Res.* **92** 1489-1496.